Available online at www.sciencedirect.com
SCIENCE DIRECT®
ELSEVIER
International Journal of Solids and Structures 42 (2005) 6376–6408
INTERNATIONAL JOURNAL OF SOLIDS and STRUCTURES
www.elsevier.com/locate/ijsolstr

On the investigation of elasticity equation for orthotropic materials and the solution of the associated scattering problem

K.A. Anagnostopoulos, A. Charalambopoulos *, C.V. Massalas

Department of Material Science and Engineering, University of Ioannina, 45110 Ioannina, Greece

Received 14 July 2004; received in revised form 6 May 2005
Available online 27 June 2005

Abstract

The present work concerns the investigation of the two-dimensional direct scattering problem of time-harmonic elastic waves from bounded anisotropic components of isotropic media. We obtain a Fourier series expansion for the elastic field in the interior of the anisotropic inclusion based on a suitable diagonalization applied to the underlying differential system and a plane wave expansion of the sought field, provided that the inclusion exhibits orthotropic symmetry. This expansion is then exploited to acquire a semi-analytical solution to the associated elastic transmission scattering problem. Numerical results for several geometric configurations and varying degree of anisotropy are presented revealing the pronounced effect of the specific anisotropic character on the scattering mechanism.

Keywords: Anisotropic elasticity; Transmission scattering problem

1. Introduction

In recent decades, the solution of physical problems involving anisotropic media has received great deal of attention since the anisotropic character is of paramount concern in many fields of scientific interest. In particular, the study of wave propagation and scattering of elastic waves in anisotropic media is related to nondestructive testing, materials characterization at both microscale (e.g., crystals and polycrystals) and macroscale level (e.g., fiber-reinforced composite materials), seismic theory etc. From a theoretical point of view, the development of a theoretical model describing the scattering process from anisotropic materials

* Corresponding author. Tel.: +30 26510 97149; fax: +30 26510 97072.
E-mail addresses: acharala@cc.uoi.gr (A. Charalambopoulos), massalas@cc.uoi.gr (C.V. Massalas).

0020-7683/$ - see front matter © 2005 Elsevier Ltd. All rights reserved.
doi:10.1016/j.ijsolstr.2005.05.004

constitutes a very interesting mathematical problem with several complication factors due to the direction dependence, which characterizes the mechanical behavior of the material. Moreover, such a model is regarded as an indispensable tool in the analysis of more complicated structures related to a number of engineering applications. Examples include the quantitative evaluation through a model analyzing the scattering from the sample when the immersion ultrasonic technique is employed, and the stiffness and stress analysis of an individual lamina (being a constituent of a composite laminate) subjected to forces in its own plane. The restricted availability of such models for anisotropic elastic scattering is the motivation for the present work.

Generally speaking, the anisotropy level of the investigated medium, i.e., its symmetry class, dictates the degree up to which the performance of any analytical calculations is feasible. For a medium exhibiting a high degree of symmetry, e.g., transverse isotropy, analytic or semi-analytic solutions become available. Examples of two-dimensional scattering problems involving such media are Mattsson (1994, 1995) and Rajapakse and Gross (1995) where scattering by a strip-like crack and a cavity is investigated, respectively. In three dimensions, scattering by transversely isotropic cylinders is studied in Honarvar and Sinclair (1996) and Niklasson and Datta (1998) among others, while an extension of the methodology proposed in Honarvar and Sinclair (1996) to the case of a cylindrical shell is found in Kim and Ih (2003). Other examples of scattering problems involving transversely isotropic solids are Kundu and Boström (1992) and Mal et al. (1992). On the other hand, when it comes to materials with a higher degree of anisotropy, the investigation of the wave propagation and scattering phenomena is based upon numerical methods such as the finite element method (FEM; Lord et al., 1990), the elastodynamic finite integration technique (EFIT; Fellinger et al., 1995), the boundary element method (BEM; Wang et al., 1996) and the strip element method (SEM; Liu and Achenbach, 1995).

The aim of this paper is to perform a theoretical investigation of the equations governing the elastic deformations of an orthotropic material in two dimensions with the objective of describing the underlying displacement field through a Fourier series expansion, to exploit the deduced expansion towards the semi-analytical solution of the associated elastic transmission scattering problem under plane wave excitation and to exemplify the effect of the underlying anisotropic character on the scattering procedure through some numerical results.

The plan of the work at hand is as follows. The analysis of the partial differential equations describing the vibration of an elastic solid exhibiting orthotropic symmetry under a plain stress state is the subject matter of Section 2. The decoupling of the coupled differential system of elasticity equations is accomplished through an appropriate diagonalization procedure and the adoption of a plane wave expansion of the sought solutions. The main outcome of this section is a Fourier series expansion for the elastic displacement field in the orthotropic medium. In Section 3, the two-dimensional transmission scattering problem of time-harmonic elastic plane waves from an orthotropic inclusion embedded in an isotropic background medium is formulated. The semi-analytical solution of this well-posed boundary value problem is reached by performing a Navier eigenvectors expansion of the scattered displacement field (Ben-Menahem and Singh, 1981), utilizing the obtained Fourier-type expansion for the description of the elastic field in the interior of the anisotropic scatterer and requiring the satisfaction of the transmission boundary conditions on the anisotropy's surface for the involved displacement fields. In the numerical examples in Section 4, we study the elastic response of an anisotropic solid exhibiting cubic symmetric behavior, for varying degree of cubic anisotropy and several geometric cross-sections of the scatterer upon observing both far-field and near-field quantities.

2. Investigation of the equation of orthotropic elasticity

The equations of elasticity describe the motion of an elastic medium in terms of an elastic displacement vector $\boldsymbol{U} : G \to \mathbb{R}^2$ and a stress tensor (σ_{jk}), $j,k = 1,2$. Assuming the usual tensor summation convention, stress and strain are connected by means of Hooke's law

$$\sigma_{jk} = C_{jkmn} U_{mn}, \quad j,k,m,n = 1,2, \tag{1}$$

while the components of the strain tensor in terms of the displacement field are

$$U_{mn} := \tfrac{1}{2}(\partial_m U_n + \partial_n U_m), \quad m,n = 1,2, \tag{2}$$

where ∂_m indicates the partial derivative with respect to the coordinate x_m, $m = 1,2$ of a Cartesian system $O(x_1,x_2)$. The elastic moduli $C_{jkmn}, j,k,m,n = 1,2$, which characterize the stiffness properties of the material occupying region G are, in general, real-valued, bounded and measurable functions on G and satisfy the following symmetry relations:

$$C_{jkmn} = C_{mnjk} = C_{kjmn}, \quad j,k,m,n = 1,2. \tag{3}$$

It is noticed, however, that the rest of the present study deals only with the constant elastic moduli case. In addition, the elastic moduli share coercivity properties expressed by the relation

$$\exists c > 0, \qquad \forall \xi_{jk} \in \mathbb{C}, \;\; \xi_{jk} = \xi_{kj}, \quad \xi_{jk} C_{jkmn} \overline{\xi}_{mn} \geqslant c \sum_{j=1}^{2} \sum_{k=1}^{2} |\xi_{jk}|^2, \tag{4}$$

where the overbar indicates complex conjugation.

Adopting the terminology presented in Leis (1986), we use the Sommerfeld symbolism for the stresses and strains defining

$$\alpha_1 := \sigma_{11}, \quad \alpha_2 := \sigma_{22}, \quad \alpha_3 := \sigma_{12},$$
$$\varepsilon_1 := U_{11}, \quad \varepsilon_2 := U_{22}, \quad \varepsilon_3 := 2U_{12},$$

thus obtaining the alternative form of Hooke's law

$$\alpha_j = Q_{jk} \varepsilon_k, \quad j,k = 1,2,3, \tag{5}$$

where we have introduced the 3×3 symmetric positive definite stiffness matrix

$$Q := \begin{bmatrix} C_{1111} & C_{1122} & C_{1112} \\ \cdot & C_{2222} & C_{2212} \\ \cdot & \cdot & C_{1212} \end{bmatrix}. \tag{6}$$

We remark that the orthotropic medium under consideration is completely characterized by four independent stiffness coefficients C_{1111}, C_{1122}, C_{2222}, C_{1212}, while the remaining elastic moduli are assigned the values $C_{1112} = C_{2212} = 0$. Therefore matrix Q can also be written as follows:

$$Q = \begin{bmatrix} Q_{11} & Q_{12} & 0 \\ Q_{12} & Q_{22} & 0 \\ 0 & 0 & Q_{66} \end{bmatrix}, \tag{7}$$

where the specific values of its entries in terms of the elastic moduli follow by inspection by taking into account that the Voigt's contracted notation Q_{66} has been used for the relative shear stiffness corresponding to the entry Q_{33}. It is also noted that Eq. (5) with Q defined by Eq. (7) correspond to the stress–strain relations in coordinates aligned with principal material directions for a plane stress state of an orthotropic material (Jones, 1975). Moreover, the assumption of vanishing coefficients C_{1112} and C_{2212} is by no means a restrictive one since the general case where the coordinate system is not aligned with the principal directions of the material can be obtained if a rotation is introduced. The degenerate case of an isotropic medium is obtained in case that $Q_{11} = Q_{12} + 2Q_{66}$ and $Q_{22} = Q_{11}$. In addition, the requirement of positive definiteness for Q implies that $Q_{11}, Q_{22}, Q_{66} > 0$ and $|Q_{12}| < \sqrt{Q_{11}Q_{22}}$ and the coercivity property (4) leads to

$Q_{12} < \frac{1}{2}(Q_{11} + Q_{22})$. The componentwise form of the equations of elasticity in the case where no exterior forces apply on region G is

$$\rho \ddot{U}_j - \partial_k \sigma_{jk} = 0, \quad j,k = 1,2, \tag{8}$$

where ρ is the material density and the overdot symbol indicates time differentiation. Assuming that the anisotropic medium undergoes harmonic oscillation of the form $e^{-i\omega t}$ with angular frequency ω, Eqs. (8) reduce to the homogeneous, time-reduced, coupled system of elasticity equations

$$Q_{11}\partial_1^2 U_1 + (Q_{12} + Q_{66})\partial_1\partial_2 U_2 + Q_{66}\partial_2^2 U_1 + \rho\omega^2 U_1 = 0, \tag{9}$$

$$Q_{66}\partial_1^2 U_2 + (Q_{12} + Q_{66})\partial_1\partial_2 U_1 + Q_{22}\partial_2^2 U_2 + \rho\omega^2 U_2 = 0. \tag{10}$$

Decoupling this differential system is equivalent to consider the following eigenvalue problem:

$$\begin{bmatrix} Q_{11}\partial_1^2 + Q_{66}\partial_2^2 + \rho\omega^2 - \lambda & (Q_{12} + Q_{66})\partial_1\partial_2 \\ (Q_{12} + Q_{66})\partial_1\partial_2 & Q_{66}\partial_1^2 + Q_{22}\partial_2^2 + \rho\omega^2 - \lambda \end{bmatrix} \begin{pmatrix} U_1^{(\lambda)} \\ U_2^{(\lambda)} \end{pmatrix} = \begin{pmatrix} 0 \\ 0 \end{pmatrix}, \tag{11}$$

where λ stands for a suitable differential operator to be determined shortly and $(U_1^{(\lambda)} U_2^{(\lambda)})^\top$ is the corresponding eigenvector with the superscript '$\top$' denoting transposition. Demanding from the determinant of the matrix in Eq. (11) to vanish we obtain

$$\lambda^2 - \left[(Q_{11} + Q_{66})\partial_1^2 + (Q_{22} + Q_{66})\partial_2^2 + 2\rho\omega^2\right]\lambda + (Q_{11}\partial_1^2 + Q_{66}\partial_2^2 + \rho\omega^2)(Q_{66}\partial_1^2 + Q_{22}\partial_2^2 + \rho\omega^2) - (Q_{12} + Q_{66})^2\partial_1^2\partial_2^2 = 0. \tag{12}$$

After straightforward manipulations, one can show that the discriminant d of the above quadratic equation in λ is equal to the following differential operator

$$d = d(\partial_1, \partial_2) = \left[(Q_{11} - Q_{66})\partial_1^2 + (Q_{22} - Q_{66})\partial_2^2\right]^2 - 4S\partial_1^2\partial_2^2, \tag{13}$$

where

$$S := (Q_{11} - Q_{66})(Q_{22} - Q_{66}) - (Q_{12} + Q_{66})^2. \tag{14}$$

It is to be noticed that dealing with an isotropic medium implies the vanishing of the parameter S, a fact frequently used in the subsequent analysis. By evoking Fourier transform arguments, the application of the operator d on every function $f(\boldsymbol{r})$, $\boldsymbol{r} \in \mathbb{R}^2$, which belongs to its domain can be expressed through the relation

$$df(\boldsymbol{r}) := \int_{\mathbb{R}^2} \mathrm{d}\boldsymbol{k}\, d(ik_1, ik_2) e^{i\boldsymbol{k}\cdot\boldsymbol{r}} \hat{f}(\boldsymbol{k}), \tag{15}$$

where $\boldsymbol{k} := (k_1, k_2)$ and $\hat{f}(\boldsymbol{k})$ stands for the Fourier transform of $f(\boldsymbol{r})$ defined by

$$\hat{f}(\boldsymbol{k}) := \frac{1}{(2\pi)^2} \int_{\mathbb{R}^2} \mathrm{d}\boldsymbol{r}\, e^{-i\boldsymbol{k}\cdot\boldsymbol{r}} f(\boldsymbol{r}). \tag{16}$$

We remark that the symbol $d(ik_1, ik_2)$ can be decomposed as follows:

$$d(ik_1, ik_2) = d_1(k_1, k_2) d_2(k_1, k_2), \tag{17}$$

where

$$d_1(k_1, k_2) := (Q_{11} - Q_{66})k_1^2 + (Q_{22} - Q_{66})k_2^2 + 2\sqrt{S}k_1k_2, \tag{18}$$

$$d_2(k_1, k_2) := (Q_{11} - Q_{66})k_1^2 + (Q_{22} - Q_{66})k_2^2 - 2\sqrt{S}k_1k_2. \tag{19}$$

In view of (17)–(19), one can immediately verify with the aid of (14) that $d(\mathrm{i}k_1, \mathrm{i}k_2) > 0$ for every pair $(k_1, k_2) \in \mathbb{R}^2$. Consequently, the operator d has positive symbol and is clearly positive definite. We are then able to define the square root operator $\sqrt{d}$ as follows:

$$\sqrt{d} f(\boldsymbol{r}) := \int_{\mathbb{R}^2} \mathrm{d}\boldsymbol{k} \sqrt{d(\mathrm{i}k_1, \mathrm{i}k_2)} \mathrm{e}^{\mathrm{i}\boldsymbol{k}\cdot\boldsymbol{r}} \hat{f}(\boldsymbol{k}), \tag{20}$$

and proceed with the solution of the operational quadratic equation (12). This procedure leads to the determination of the eigenvalue operators λ_i, $i = 1, 2$,

$$\lambda_{1,2} := \tfrac{1}{2}\left[(Q_{11} + Q_{66})\partial_1^2 + (Q_{22} + Q_{66})\partial_2^2 + 2\rho\omega^2 \pm \sqrt{d}\right], \tag{21}$$

which in the isotropic limit become $\lambda_1 = Q_{11}\Delta + \rho\omega^2$ and $\lambda_2 = Q_{66}\Delta + \rho\omega^2$, referring to the well known Helmholtz differential operators concerning the longitudinal and transverse elastic waves, respectively.

Let $U := (U_1 \;\; U_2)^\top$ be a solution of the system (9) and (10). Then the field U is represented as

$$U = PV, \tag{22}$$

where

$$P := \begin{bmatrix} U_1^{(\lambda_1)} & U_1^{(\lambda_2)} \\ U_2^{(\lambda_1)} & U_2^{(\lambda_2)} \end{bmatrix}, \tag{23}$$

is the eigenvector matrix and $V := (V_1 \;\; V_2)^\top$ is an auxiliary field whose components V_i, $i = 1, 2$ are solutions of the decoupled equations $\lambda_1 V_1 = 0$ and $\lambda_2 V_2 = 0$, which in complete form are

$$\left[(Q_{11} + Q_{66})\partial_1^2 + (Q_{22} + Q_{66})\partial_2^2 + 2\rho\omega^2 + \sqrt{d}\right] V_1 = 0, \tag{24}$$

$$\left[(Q_{11} + Q_{66})\partial_1^2 + (Q_{22} + Q_{66})\partial_2^2 + 2\rho\omega^2 - \sqrt{d}\right] V_2 = 0. \tag{25}$$

In order to determine the functions V_i, $i = 1, 2$, we first exploit the commuting property of λ_i, $i = 1, 2$, which assures that $\lambda_1\lambda_2 V_i = 0$, $i = 1, 2$. Defining the operator L by

$$L := \lambda_1\lambda_2 = \left[(Q_{11} + Q_{66})\partial_1^2 + (Q_{22} + Q_{66})\partial_2^2 + 2\rho\omega^2\right]^2 - d, \tag{26}$$

one can show that the determination of the sought functions V_i, $i = 1, 2$ satisfying $\lambda_i V_i = 0$, $i = 1, 2$ reduces to the solution of the fourth-order scalar differential equation $L\Psi = 0$. Indeed, for every Ψ satisfying $L\Psi = 0$, we easily verify that $W_1 := \lambda_2\Psi$ (resp. $W_2 := \lambda_1\Psi$) satisfies the equation $\lambda_1 W_1 = 0$ (resp. $\lambda_2 W_2 = 0$) and therefore the pair $(W_1 \;\; W_2)^\top$ is a suitable candidate pair of functions for the sought pair of solutions $(V_1 \;\; V_2)^\top$. We postpone the treatment of equation $L\Psi = 0$ and proceed with the implementation of the transformation induced by Eq. (22). Adopting the reasonable symbol correspondence $\lambda_1 \iff (+)$ and $\lambda_2 \iff (-)$ we find from (11) that

$$\left[\frac{Q_{11} - Q_{66}}{2}\partial_1^2 + \frac{Q_{66} - Q_{22}}{2}\partial_2^2 \mp \frac{\sqrt{d}}{2}\right] U_1^{(\pm)} + (Q_{12} + Q_{66})\partial_1\partial_2 U_2^{(\pm)} = 0. \tag{27}$$

Consequently, the matrix P given in Eq. (23) can be selected as follows:

$$P = \begin{bmatrix} (Q_{12} + Q_{66})\partial_1\partial_2 & -(Q_{12} + Q_{66})\partial_1\partial_2 \\ \frac{Q_{66} - Q_{11}}{2}\partial_1^2 + \frac{Q_{22} - Q_{66}}{2}\partial_2^2 + \frac{\sqrt{d}}{2} & \frac{Q_{11} - Q_{66}}{2}\partial_1^2 + \frac{Q_{66} - Q_{22}}{2}\partial_2^2 + \frac{\sqrt{d}}{2} \end{bmatrix} R, \tag{28}$$

where R is an arbitrary linear operator commuting with the differential operators appeared in the entries of the matrix P (actually R can be considered as part of a redefined vector V). The transformation (22) now reads

$$U_1 = (Q_{12} + Q_{66})\partial_1\partial_2 R(V_1 - V_2), \tag{29}$$

$$U_2 = \left[\frac{Q_{66} - Q_{11}}{2}\partial_1^2 + \frac{Q_{22} - Q_{66}}{2}\partial_2^2\right] R(V_1 - V_2) + \frac{\sqrt{d}}{2} R(V_1 + V_2). \tag{30}$$

Given that $V_1 = \lambda_2 \Psi$ and $V_2 = \lambda_1 \Psi$, where Ψ solves $L\Psi = 0$, we have

$$(V_1 - V_2) = -\sqrt{d}\Psi, \tag{31}$$

$$(V_1 + V_2) = \left[(Q_{11} + Q_{66})\partial_1^2 + (Q_{22} + Q_{66})\partial_2^2 + 2\rho\omega^2\right]\Psi. \tag{32}$$

Selecting $R := (1/(Q_{12} + Q_{66}))(\sqrt{d})^{-1}$, with the operator $(\sqrt{d})^{-1}$ defined through the relation

$$(\sqrt{d})^{-1} f(\boldsymbol{r}) := \int_{\mathbb{R}^2} \mathrm{d}\boldsymbol{k}\, \frac{1}{\sqrt{d(\mathrm{i}k_1, \mathrm{i}k_2)}} \mathrm{e}^{\mathrm{i}\boldsymbol{k}\cdot\boldsymbol{r}} \hat{f}(\boldsymbol{k}), \tag{33}$$

we obtain the differential representation

$$U_1 = -\partial_1\partial_2\Psi, \tag{34}$$

$$U_2 = (Q_{12} + Q_{66})^{-1}(Q_{11}\partial_1^2 + Q_{66}\partial_2^2 + \rho\omega^2)\Psi. \tag{35}$$

It is easily verified that the pair (34) and (35) satisfies the coupled differential system of elasticity (9) and (10) with $\Psi \in \mathrm{Ker}\, L$. In addition, this differential representation in the isotropic limit reduces to the well-known Helmholtz decomposition

$$\begin{pmatrix} U_1 \\ U_2 \end{pmatrix} = \begin{pmatrix} U_1^{\mathrm{p}} \\ U_2^{\mathrm{p}} \end{pmatrix} + \begin{pmatrix} U_1^{\mathrm{s}} \\ U_2^{\mathrm{s}} \end{pmatrix} = \nabla\Psi^{\mathrm{p}} + \nabla \times (\Psi^{\mathrm{s}}\hat{\boldsymbol{x}}_3), \tag{36}$$

where $\hat{\boldsymbol{x}}_3$ denotes a unit vector perpendicular to the x_1x_2-plane.

As far as the investigation of the fourth-order scalar differential equation $L\Psi = 0$ is concerned, we first note that in the degenerate case of an isotropic medium, that is, $Q_{11} = Q_{12} + 2Q_{66}$ and $Q_{22} = Q_{11}$, the operator L simplifies to $L_{\mathrm{isotr.}} := 4(Q_{11}\Delta + \rho\omega^2)(Q_{66}\Delta + \rho\omega^2)$ and hence its kernel consists of all the solutions of two scalar Helmholtz equations with different wave numbers. Thus an appropriate basis for $\mathrm{Ker}L_{\mathrm{isotr.}}$ consists of the set $\{X_m(k_t r)\mathrm{e}^{\mathrm{i}m\varphi}, m \in \mathbb{Z}, t = \mathrm{p}, \mathrm{s}\}$, where (r, φ) are the polar coordinates, $k_{\mathrm{p}} := \omega\sqrt{\rho/Q_{11}}$, $k_{\mathrm{s}} := \omega\sqrt{\rho/Q_{66}}$ and X_m vary over the possible alternatives of the Bessel or Hankel functions of the first and second kind and integer order. On the other hand, in the general anisotropic case, the rotation invariant character of the corresponding isotropic operator is no longer preserved and this fact is expected to have an impact on the symmetries of the sought solutions. The polar geometry is not the convenient configuration any more since the elements of the aforementioned basis fail to annihilate the L operator for any value of the wave number k_t. For this reason we proceed by seeking solutions expressed via plane waves of the form $\mathrm{e}^{-\mathrm{i}k\hat{\boldsymbol{k}}\cdot\boldsymbol{r}}$, where $\boldsymbol{r} := (x_1, x_2)$ is the position vector and $\hat{\boldsymbol{k}} := (\cos u, \sin u)$, $u \in [0, 2\pi)$ is the plane wave propagation unit vector. Forcing the plane waves $\mathrm{e}^{-\mathrm{i}k\hat{\boldsymbol{k}}\cdot\boldsymbol{r}}$ to belong to $\mathrm{Ker}\, L$, that is,

$$0 = \left\{\left[(Q_{11} + Q_{66})\partial_1^2 + (Q_{22} + Q_{66})\partial_2^2 + 2\rho\omega^2\right]^2 - \left[(Q_{11} - Q_{66})\partial_1^2 + (Q_{22} - Q_{66})\partial_2^2\right]^2 - 4S\partial_1^2\partial_2^2\right\}\{\mathrm{e}^{-\mathrm{i}k\hat{\boldsymbol{k}}\cdot\boldsymbol{r}}\}, \tag{37}$$

we find that

$$\begin{aligned} 0 = {} & \left\{Q_{11}Q_{66}\cos^4 u + Q_{22}Q_{66}\sin^4 u + [(Q_{11} + Q_{22})Q_{66} + S]\cos^2 u \sin^2 u\right\}k^4 \\ & - \rho\omega^2\left\{(Q_{11} + Q_{66})\cos^2 u + (Q_{22} + Q_{66})\sin^2 u\right\}k^2 + \rho^2\omega^4. \end{aligned} \tag{38}$$

Solving the last equation, which constitutes the dispersion relation for the underlying orthotropic medium, in terms of the wave number k we obtain

$$k^2 = k_{\pm}^2(u) = \rho\omega^2 \frac{(Q_{11}+Q_{66})\cos^2 u + (Q_{22}+Q_{66})\sin^2 u \pm \sqrt{D_1(u)}}{2D_2(u)}, \tag{39}$$

where

$$D_1(u) := \left[(Q_{11}-Q_{66})\cos^2 u + (Q_{22}-Q_{66})\sin^2 u\right]^2 - 4S\cos^2 u \sin^2 u, \tag{40}$$

and

$$D_2(u) := Q_{11}Q_{66}\cos^4 u + Q_{22}Q_{66}\sin^4 u + [(Q_{11}+Q_{22})Q_{66} + S]\cos^2 u \sin^2 u. \tag{41}$$

The expected functional dependence of the wave numbers $k_{\pm}(u)$ on the propagation direction cosines is obvious in (39). Moreover, the established constraints on the values of the elastic moduli assure that $D_1, D_2 > 0$ and the nominator in (39) is always greater than zero.

The analysis above provides with plane-wave type solutions for the equation $L\Psi = 0$. By superposing these solutions over the interval $[0, 2\pi)$ with square integrable amplitudes, one can form the set $\mathcal{Q}$ of anisotropic plane wave solutions as follows:

$$\begin{aligned}\mathcal{Q} &= \Big\{ \phi : \mathbb{R}^2 \to \mathbb{C},\ \ \phi \in C^{\infty}(\mathbb{R}^2) \ \text{ and } \ \phi(\boldsymbol{r}) \\ &= \int_0^{2\pi} \left[A_+(u)\mathrm{e}^{-\mathrm{i}k_+(u)\hat{\boldsymbol{k}}\cdot\boldsymbol{r}} + A_-(u)\mathrm{e}^{-\mathrm{i}k_-(u)\hat{\boldsymbol{k}}\cdot\boldsymbol{r}}\right] \mathrm{d}u \ \text{ for } A_{\pm} \in L^2(0,2\pi)\Big\},\end{aligned} \tag{42}$$

where $k_{\pm}(u)$ are given by the square roots of the right-hand side of Eq. (39). The establishment of the fact that every regular solution of the scalar differential equation $L\Psi = 0$ can be considered either as a member of the set $\mathcal{Q}$ or the appropriate limit of functions belonging to $\mathcal{Q}$ is an issue deserving special attention. The specific assertion has been proved to be valid in the isotropic case, when the set $\mathcal{Q}$ contains exactly the well-known Herglotz wave functions (Colton and Kress, 1992, 2001), which approximate at least in L^2-norm every solution of $L_{\text{isotr.}}\Psi = 0$ since the latter equation is decomposed in two scalar Helmholtz equations.

More precisely, in the isotropic case, the obvious reductions $k = k_{\mathrm{p(s)}} = \omega\sqrt{\rho/Q_{11}}(\omega\sqrt{\rho/Q_{66}})$ (independent of the propagation direction) hold and the general solution $\Psi(\boldsymbol{r})$, in interior domains containing the origin O, can be proved to constitute the limit in L^2-norm of the Herglotz plane-wave solutions (Colton and Kress, 2001). In this context we consider the Fourier series expansions for the amplitudes $A_t(u)$, $t = \mathrm{p}, \mathrm{s}$ as follows:

$$A_-(u)(:= A_{\mathrm{p}}(u)) = \frac{1}{2\pi}\sum_{m\in\mathbb{Z}} A_m\, \mathrm{i}^{-m}\mathrm{e}^{\mathrm{i}mu}, \tag{43}$$

$$A_+(u)(:= A_{\mathrm{s}}(u)) = \frac{1}{2\pi}\sum_{m\in\mathbb{Z}} B_m\, \mathrm{i}^{-m}\mathrm{e}^{\mathrm{i}mu}, \tag{44}$$

where A_m, B_m are arbitrary constants. Exploiting the integral representation (Morse and Feshbach, 1953)

$$J_m(kr)\mathrm{e}^{\mathrm{i}m\varphi} = \frac{1}{2\pi\mathrm{i}^m}\int_0^{2\pi} \mathrm{e}^{-\mathrm{i}k\hat{\boldsymbol{k}}\cdot\boldsymbol{r}}\mathrm{e}^{\mathrm{i}mu}\,\mathrm{d}u, \tag{45}$$

where $J_m(kr)$ are the Bessel functions of the first kind, we find that

$$\Psi(\boldsymbol{r}) = \sum_{m\in\mathbb{Z}} A_m J_m(k_{\mathrm{p}}r)\mathrm{e}^{\mathrm{i}m\varphi} + \sum_{m\in\mathbb{Z}} B_m J_m(k_{\mathrm{s}}r)\mathrm{e}^{\mathrm{i}m\varphi}, \tag{46}$$

which is recognized as the usual Bessel–Fourier expansion of interior Helmholtz equation solutions in polar coordinates. According to our previous comments, Eq. (46) holds in the L^2-sense.

However, in the anisotropic case, the above results have to be reexamined in order for every solution Ψ of $L\Psi = 0$ to be expanded in terms of the anisotropic plane waves, that is,

$$\Psi(\boldsymbol{r}) = \int_0^{2\pi} \left[A_+(u) \mathrm{e}^{-\mathrm{i}k_+(u)\hat{\boldsymbol{k}}\cdot\boldsymbol{r}} + A_-(u) \mathrm{e}^{-\mathrm{i}k_-(u)\hat{\boldsymbol{k}}\cdot\boldsymbol{r}} \right] \mathrm{d}u, \tag{47}$$

where equality is equivalent to convergence in an appropriate functional space. The integrals appearing in the right-hand side of Eq. (47) can be considered as generalized 'anisotropic' Herglotz functions and hence one has to establish the denseness of these functions in the space of solutions of $L\Psi = 0$. The basic arguments assuring the completeness of the anisotropic plane wave functions have been developed by the authors and presented in Appendix A. This completeness result assures that the solution $\Psi(\boldsymbol{r})$ can be represented as

$$\Psi(\boldsymbol{r}) = \sum_{m\in\mathbb{Z}} A_m^+ \frac{1}{2\pi \mathrm{i}^m} \int_0^{2\pi} \mathrm{e}^{-\mathrm{i}k_+(u)\hat{\boldsymbol{k}}\cdot\boldsymbol{r}} \mathrm{e}^{\mathrm{i}mu} \mathrm{d}u + \sum_{m\in\mathbb{Z}} A_m^- \frac{1}{2\pi \mathrm{i}^m} \int_0^{2\pi} \mathrm{e}^{-\mathrm{i}k_-(u)\hat{\boldsymbol{k}}\cdot\boldsymbol{r}} \mathrm{e}^{\mathrm{i}mu} \mathrm{d}u. \tag{48}$$

Based on this representation, the Cartesian components of the sought elastic field $\boldsymbol{U} := (U_1, U_2)$ given by Eqs. (34) and (35) assume the following Fourier series expansions:

$$U_1(\boldsymbol{r}) = \frac{1}{4\mathrm{i}} \sum_{\pm} \sum_{m\in\mathbb{Z}} A_m^{\pm} \left\{ \Theta_{m-2}^{\pm}(\boldsymbol{r}) - \Theta_{m+2}^{\pm}(\boldsymbol{r}) \right\}, \tag{49}$$

$$U_2(\boldsymbol{r}) = \frac{1}{(Q_{12}+Q_{66})} \sum_{\pm} \sum_{m\in\mathbb{Z}} A_m^{\pm} \left\{ \rho\omega^2 \Phi_m^{\pm}(\boldsymbol{r}) - \frac{(Q_{11}+Q_{66})}{2} \Theta_m^{\pm}(\boldsymbol{r}) + \frac{(Q_{11}-Q_{66})}{4} \left[\Theta_{m-2}^{\pm}(\boldsymbol{r}) + \Theta_{m+2}^{\pm}(\boldsymbol{r}) \right] \right\}, \tag{50}$$

where the symbol $\sum_{\pm}$ indicates summation over both (+) and (−) quantities and the basic functions $\Phi_m^{\pm}(\boldsymbol{r})$ and $\Theta_m^{\pm}(\boldsymbol{r})$ are defined by the following integral expressions:

$$\Phi_m^{\pm}(\boldsymbol{r}) := \frac{1}{2\pi \mathrm{i}^m} \int_0^{2\pi} \mathrm{e}^{-\mathrm{i}k_{\pm}(u)\hat{\boldsymbol{k}}\cdot\boldsymbol{r}} \mathrm{e}^{\mathrm{i}mu} \mathrm{d}u, \tag{51}$$

$$\Theta_m^{\pm}(\boldsymbol{r}) := \frac{1}{2\pi \mathrm{i}^m} \int_0^{2\pi} k_{\pm}^2(u) \mathrm{e}^{-\mathrm{i}k_{\pm}(u)\hat{\boldsymbol{k}}\cdot\boldsymbol{r}} \mathrm{e}^{\mathrm{i}mu} \mathrm{d}u. \tag{52}$$

We notice here that the u-dependence of the wave numbers complicates the performance of the integrations appearing in Eqs. (51) and (52). An analytical approach treating these integrals based on complex analysis integration arguments, that is, substitution $z = \mathrm{e}^{\mathrm{i}u}$ and application of Cauchy integral techniques to the resulted integral on the unit circle of the complex plane has been attempted. Unfortunately, it can be shown that the appearance of the square roots in $k_{\pm}(z)$ results in several branch points both inside and outside the unit circle thus rendering the performance of the complex integration a difficult task, which can be alleviated only in the asymptotic analysis region since steepest descent arguments can then be evoked. Unambiguously, an asymptotic analysis approach would restrict radically both the physical and the geometrical framework of our problem. In contrast, the employment of a simple numerical integration scheme, e.g., a trapezoidal rule approximation, performed easily on the interval $[0, 2\pi)$, turns out to be a rational choice leading to very accurate representations of the basis functions, which are very exploitable from the application point of view. In the forthcoming numerical examples such an approach is implemented.

3. Scattering by a two-dimensional orthotropic inclusion

In the sequel, our previous theoretical results concerning the Fourier series expansion of the elastic displacement field in an anisotropic material exhibiting orthotropic symmetry are exploited in order to solve a specific boundary value problem (BVP), namely the elastic transmission scattering problem. In particular, we consider the two-dimensional scattering problem of the elastic plane waves $\boldsymbol{u}^{\mathrm{inc}}(\boldsymbol{r})$ from an orthotropic scatterer occupying region G, which is characterized by the fourth-order stiffness tensor $\widetilde{\boldsymbol{C}} = C_{jkmn}\hat{\boldsymbol{x}}_j \otimes \hat{\boldsymbol{x}}_k \otimes \hat{\boldsymbol{x}}_m \otimes \hat{\boldsymbol{x}}_n$, $j,k,m,n = 1,2$ (the symbol '$\otimes$' denotes juxtaposition of two unit vectors) and the material density ρ_{int} and is embedded in an isotropic background medium with Lamé constants λ, μ and mass density ρ_{ext}. In mathematical terms, the transmission scattering problem can be formulated as a task of determining the scattered field $\boldsymbol{u}^{\mathrm{sct}} \in [C^2(\mathbb{R}^2 \setminus \overline{G})]^2 \cap [C^1(\mathbb{R}^2 \setminus G)]^2$ and the interior field $\boldsymbol{u}^{\mathrm{int}} \in [C^2(G)]^2 \cap [C^1(\overline{G})]^2$ such that

$$\nabla \cdot [\widetilde{\boldsymbol{C}} : \nabla \boldsymbol{u}^{\mathrm{int}}(\boldsymbol{r})] + \rho_{\mathrm{int}}\omega^2 \boldsymbol{u}^{\mathrm{int}}(\boldsymbol{r})\boldsymbol{0}, \quad \boldsymbol{r} \in G, \tag{53}$$

$$\Delta^* \boldsymbol{u}^{\mathrm{sct}}(\boldsymbol{r}) + \rho_{\mathrm{ext}}\omega^2 \boldsymbol{u}^{\mathrm{sct}}(\boldsymbol{r}) = \boldsymbol{0}, \quad \boldsymbol{r} \in \mathbb{R}^2 \setminus \overline{G}, \tag{54}$$

$$\boldsymbol{u}^{\mathrm{int}}(\boldsymbol{r}) - \boldsymbol{u}^{\mathrm{sct}}(\boldsymbol{r}) = \boldsymbol{f}(\boldsymbol{r}), \quad \boldsymbol{r} \in \partial G, \tag{55}$$

$$\hat{\boldsymbol{v}} \cdot \widetilde{\boldsymbol{C}} : \nabla \boldsymbol{u}^{\mathrm{int}}(\boldsymbol{r}) - \boldsymbol{T}_{\mathrm{ext}} \boldsymbol{u}^{\mathrm{sct}}(\boldsymbol{r}) = \boldsymbol{h}(\boldsymbol{r}), \quad \boldsymbol{r} \in \partial G, \tag{56}$$

$$\lim_{r\to\infty} \sqrt{r}\left(\frac{\partial \boldsymbol{u}_t^{\mathrm{sct}}(\boldsymbol{r})}{\partial r} - \mathrm{i}k_t^{\mathrm{ext}} \boldsymbol{u}_t^{\mathrm{sct}}(\boldsymbol{r})\right) = \boldsymbol{0}, \quad t = \mathrm{p}, \mathrm{s}, \tag{57}$$

with specific data $\boldsymbol{f}(\boldsymbol{r}) := \boldsymbol{u}^{\mathrm{inc}}(\boldsymbol{r})$ and $\boldsymbol{h}(\boldsymbol{r}) := \boldsymbol{T}_{\mathrm{ext}} \boldsymbol{u}^{\mathrm{inc}}(\boldsymbol{r})$ for $\boldsymbol{r} \in \partial G$. The first two equations are the underlying differential equations with $\Delta^* := \mu\Delta + (\lambda + \mu)\nabla\nabla\cdot$, denoting the Lamé operator and ':' indicating a double contraction, i.e., $(\boldsymbol{a} \otimes \boldsymbol{b} \otimes \boldsymbol{c} \otimes \boldsymbol{d}) : (\boldsymbol{e} \otimes \boldsymbol{f}) = (\boldsymbol{d} \cdot \boldsymbol{e})(\boldsymbol{c} \cdot \boldsymbol{f})(\boldsymbol{a} \otimes \boldsymbol{b})$. Eqs. (55) and (56) represent the transmission boundary conditions (BCs) assuring displacement and stress continuity through the discontinuity surface ∂G, while Eq. (57) stands for the Kupradze (1979) radiation conditions, applying to the longitudinal and transverse parts of the scattered field $\boldsymbol{u}^{\mathrm{sct}}(\boldsymbol{r}) = \boldsymbol{u}_{\mathrm{p}}^{\mathrm{sct}}(\boldsymbol{r}) + \boldsymbol{u}_{\mathrm{s}}^{\mathrm{sct}}(\boldsymbol{r})$ and being valid uniformly over all directions $\hat{\boldsymbol{r}} := \boldsymbol{r}/|\boldsymbol{r}| = \boldsymbol{r}/r$. We also mention that $\hat{\boldsymbol{v}} \cdot \widetilde{\boldsymbol{C}} : \nabla \boldsymbol{u}^{\mathrm{int}}(\boldsymbol{r})$ is the elastic conormal derivative of the interior field $\boldsymbol{u}^{\mathrm{int}}(\boldsymbol{r})$ on ∂G, $k_{\mathrm{p}}^{\mathrm{ext}} := \omega\sqrt{\rho_{\mathrm{ext}}/(\lambda + 2\mu)}$ and $k_{\mathrm{s}}^{\mathrm{ext}} := \omega\sqrt{\rho_{\mathrm{ext}}/\mu}$ are the longitudinal and transverse wavenumbers, respectively, in the background medium, while

$$\boldsymbol{T}_{\mathrm{ext}} := 2\mu\hat{\boldsymbol{v}} \cdot \nabla + \lambda\hat{\boldsymbol{v}}\nabla \cdot + \mu\hat{\boldsymbol{v}} \times \nabla\times, \tag{58}$$

stands for the surface traction operator in terms of the outward unit normal $\hat{\boldsymbol{v}}$ on scatterer's surface.

The BVP (53)–(57) disposes a weak formulation, in which $\boldsymbol{u}^{\mathrm{sct}} \in [H^1_{\mathrm{loc}}(\mathbb{R}^2 \setminus \overline{G})]^2$, $\boldsymbol{u}^{\mathrm{int}} \in [H^1(G)]^2$ and the pair $(\boldsymbol{f}, \boldsymbol{h})$ of boundary data is in $[H^{1/2}(\partial G)]^2 \times [H^{-1/2}(\partial G)]^2$ (H^k denotes the usual Sobolev space). This more general transmission problem can actually be considered as a special case of the corresponding transmission problem examined thoroughly in Charalambopoulos (2002), where the problem of scattering by a generally anisotropic inhomogeneous inclusion in $\mathbb{R}^3$ is investigated. There it is shown that, when specific data $(\boldsymbol{f}, \boldsymbol{h})$ are prescribed on the boundary ∂G, the transmission problem (in its weak form) possesses a unique solution, i.e., a solution pair $(\boldsymbol{u}^{\mathrm{sct}}, \boldsymbol{u}^{\mathrm{int}})$, depending continuously on the surface data. This well-posedness is, of course, inherited to the transmission problem in its classical form (53)–(57) through boundary value problem's regularity theory.

For the solution of the well-posed BVP under discussion, a method based on the representation of the scattered displacement field $\boldsymbol{u}^{\mathrm{sct}}(\boldsymbol{r})$ in terms of the Navier eigenvectors is adopted. It is well known that Navier eigenvectors result from the Helmholtz decomposition and constitute a complete set of vector functions in the space of solutions of time-independent Navier equation. Hence, in the polar coordinate system (r, φ), the scattered field assumes the representation

$$\boldsymbol{u}^{\mathrm{sct}}(\boldsymbol{r}) = \sum_{m=-\infty}^{\infty} \left\{ A_m^{\mathrm{ext}} \boldsymbol{L}_m^{(3)}(\boldsymbol{r}) + B_m^{\mathrm{ext}} \boldsymbol{M}_m^{(3)}(\boldsymbol{r}) \right\}, \quad \boldsymbol{r} \in \mathbb{R}^2 \setminus \overline{G}, \tag{59}$$

in terms of the irrotational eigenvector $\boldsymbol{L}_m^{(j)}(\boldsymbol{r})$ and the solenoidal one $\boldsymbol{M}_m^{(j)}(\boldsymbol{r})$, which are defined through the relations

$$\boldsymbol{L}_m^{(l)}(\boldsymbol{r}) := \frac{1}{k_{\mathrm{p}}^{\mathrm{ext}}} \nabla \Psi_{m,\mathrm{p}}^{(l)}(\boldsymbol{r}), \tag{60}$$

$$\boldsymbol{M}_m^{(l)}(\boldsymbol{r}) := \frac{1}{k_{\mathrm{s}}^{\mathrm{ext}}} \nabla \Psi_{m,\mathrm{s}}^{(l)}(\boldsymbol{r}) \times \hat{\boldsymbol{x}}_3. \tag{61}$$

The set of scalar Helmholtz equation solutions $\{\Psi_{m,t}^{(l)}(\boldsymbol{r}), m \in \mathbb{Z}, t = \mathrm{p}, \mathrm{s}, l = 1,2,3,4\}$ is given by

$$\Psi_{m,t}^{(l)}(\boldsymbol{r}) := X_m^{(l)}(k_t^{\mathrm{ext}} r) \mathrm{e}^{\mathrm{i}m\varphi}, \tag{62}$$

while $X_m^{(l)}(kr) = \{J_m(kr), Y_m(kr), H_m^{(1)}(kr), H_m^{(2)}(kr)\}$ according as $l = 1,2,3,4$, respectively. The specific selection $l = 3$ in representation (59), which corresponds to the choice of Hankel functions of the first kind and of integer order, assures the appropriate behavior of the scattered field at infinity.

The description of the elastic displacement in the interior of the orthotropic scatterer takes advantage of the Fourier-type expansion deduced in the previous section. Exploiting Eqs. (49) and (50) and approximating the integral expressions in Eqs. (51) and (52) by a M-point trapezoidal rule, the Cartesian components of $\boldsymbol{u}^{\mathrm{int}}(\boldsymbol{r})$, $\boldsymbol{r} \in G$ are given as

$$u_1^{\mathrm{int}}(r,\varphi) = \sum\nolimits_{m'=-\infty}^{\infty} \left\{ \frac{\mathrm{i}^{-m'}}{M} \sum_{\pm} \left\{ A_{m'}^{\pm} \sum_{j=1}^{M} \left\{ k_{\pm}^2(u_j) \sin u_j \cos u_j \mathrm{e}^{-\mathrm{i}k_{\pm}(u_j) r \cos(\varphi - u_j)} \mathrm{e}^{\mathrm{i}m' u_j} \right\} \right\} \right\}, \tag{63}$$

$$u_2^{\mathrm{int}}(r,\varphi) = \sum_{m'=-\infty}^{\infty} \left\{ \frac{\mathrm{i}^{-m'}}{M} \sum_{\pm} \left\{ A_{m'}^{\pm} \sum_{j=1}^{M} \left\{ \frac{1}{Q_{12} + Q_{66}} [\rho\omega^2 - k_{\pm}^2(u_j) \times (Q_{11} \cos^2 u_j + Q_{66} \sin^2 u_j)] \mathrm{e}^{-\mathrm{i}k_{\pm}(u_j) r \cos(\varphi - u_j)} \mathrm{e}^{\mathrm{i}m' u_j} \right\} \right\} \right\}, \tag{64}$$

where $u_j = 2\pi(j-1)/M$, $j = 1, \ldots, M$.

The incident plane wave $\boldsymbol{u}^{\mathrm{inc}}(\boldsymbol{r})$, which excites the scatterer, propagates at an angle α with respect to the x_1-axis and is either of compressional type (longitudinally polarized P-wave), that is,

$$\boldsymbol{u}^{\mathrm{inc}}(\boldsymbol{r}) = (\cos\alpha \hat{\boldsymbol{x}}_1 + \sin\alpha \hat{\boldsymbol{x}}_2) \mathrm{e}^{\mathrm{i}k_{\mathrm{p}}^{\mathrm{ext}} r \cos(\varphi - \alpha)}, \tag{65}$$

or a transversely polarized shear S-wave of the form

$$\boldsymbol{u}^{\mathrm{inc}}(\boldsymbol{r}) = (-\sin\alpha \hat{\boldsymbol{x}}_1 + \cos\alpha \hat{\boldsymbol{x}}_2) \mathrm{e}^{\mathrm{i}k_{\mathrm{s}}^{\mathrm{ext}} r \cos(\varphi - \alpha)}. \tag{66}$$

The determination of the unknown coefficients A_m^{ext}, B_m^{ext}, $A_{m'}^{+}$, $A_{m'}^{-}$ entering the above expansions will be accomplished by requiring the satisfaction of the BCs (55) and (56), which actually involve four scalar equations dependent on the azimuthal angle φ, when projected on the unit vectors $\hat{\boldsymbol{x}}_1$, $\hat{\boldsymbol{x}}_2$. Obviously, Eq. (56) requires the calculation of the tractions from the scattered, the transmitted and the incident fields. The application of the surface traction operator given in (58) on the expansion (59) for the scattered field leads to

$$\begin{aligned} \boldsymbol{T}_{\mathrm{ext}} \boldsymbol{u}^{\mathrm{sct}}(\boldsymbol{r}) = \sum_{m=-\infty}^{\infty} & \left\{ \left\{ A_m^{\mathrm{ext}} [D_m^r(r,\varphi) \cos\varphi - D_m^{\varphi}(r,\varphi) \sin\varphi] + B_m^{\mathrm{ext}} [Z_m^r(r,\varphi) \cos\varphi - Z_m^{\varphi}(r,\varphi) \sin\varphi] \right\} \hat{\boldsymbol{x}}_1 \right. \\ & \left. + \left\{ A_m^{\mathrm{ext}} [D_m^r(r,\varphi) \sin\varphi + D_m^{\varphi}(r,\varphi) \cos\varphi] + B_m^{\mathrm{ext}} [Z_m^r(r,\varphi) \sin\varphi + Z_m^{\varphi}(r,\varphi) \cos\varphi] \right\} \hat{\boldsymbol{x}}_2 \right\}, \end{aligned} \tag{67}$$

where the expressions for $D^t_m(r,\varphi)$, $Z^t_m(r,\varphi)$, $t = r,\varphi$ are given in Appendix B. The elastic conormal derivative of the transmitted field $\boldsymbol{u}^{\text{int}}(\boldsymbol{r})$ on scatterer's surface is given as

$$\hat{\boldsymbol{v}}\cdot\widetilde{\boldsymbol{C}}:\nabla\boldsymbol{u}^{\text{int}}(\boldsymbol{r}) = \sum_{m'=-\infty}^{\infty}\left\{\sum_{\pm}\left\{A^{\pm}_{m'}\left[F^{\pm}_{m'}(r,\varphi)\hat{\boldsymbol{x}}_1 + G^{\pm}_{m'}(r,\varphi)\hat{\boldsymbol{x}}_2\right]\right\}\right\}, \tag{68}$$

where $F^{\pm}_{m'}(r,\varphi)$ and $G^{\pm}_{m'}(r,\varphi)$ are also described in Appendix B. Finally, the surface traction due to the incident plane wave (65) of compressional type is easily found to be

$$\boldsymbol{T}_{\text{ext}}\boldsymbol{u}^{\text{inc}}(\boldsymbol{r}) = \mathrm{i}k^{\text{ext}}_{\text{p}}\mathrm{e}^{\mathrm{i}k^{\text{ext}}_{\text{p}}r\cos(\varphi-\alpha)}\left\{\left[v_1(2\mu\cos^2\alpha+\lambda)+v_2(\mu\sin 2\alpha)\right]\hat{\boldsymbol{x}}_1 + \left[v_1(\mu\sin 2\alpha)+v_2(2\mu\sin^2\alpha+\lambda)\right]\hat{\boldsymbol{x}}_2\right\}, \tag{69}$$

while for the shear wave (66) the surface stress is

$$\boldsymbol{T}_{\text{ext}}\boldsymbol{u}^{\text{inc}}(\boldsymbol{r}) = \mathrm{i}k^{\text{ext}}_{\text{s}}\mathrm{e}^{\mathrm{i}k^{\text{ext}}_{\text{s}}r\cos(\varphi-\alpha)}\{[v_1(-\mu\sin 2\alpha)+v_2(\mu\cos 2\alpha)]\hat{\boldsymbol{x}}_1 + [v_1(\mu\cos 2\alpha)+v_2(\mu\sin 2\alpha)]\hat{\boldsymbol{x}}_2\}, \tag{70}$$

where v_1, v_2 are the Cartesian components of $\hat{\boldsymbol{v}}$.

So far, nothing has been said about the geometric characteristics of the two-dimensional scatterer. We consider two cases, namely, an elastic orthotropic inclusion of circular and elliptical cross-section. In the former case the boundary surface is determined by $r = a$, where a is the radius and the outward unit normal is simply given as $\hat{\boldsymbol{v}} = \hat{\boldsymbol{r}} = (\cos\varphi\hat{\boldsymbol{x}}_1 + \sin\varphi\hat{\boldsymbol{x}}_2)$, $\varphi\in[0,2\pi)$. In the case of an ellipse with semi-axes a_0, b_0 ($a_0 > b_0$) and hence semi-focal distance $h = \sqrt{a_0^2 - b_0^2}$, the elliptical surface is specified by $u_0 = \cosh^{-1}(a_0/h)$ and $\hat{\boldsymbol{v}} = (\sinh u_0\cos v\hat{\boldsymbol{x}}_1 + \cosh u_0\sin v\hat{\boldsymbol{x}}_2)/\sqrt{\cosh^2 u_0 - \cos^2 v}$, $v\in[0,2\pi)$ in terms of the elliptical coordinates (u,v).

Having in our disposal the expressions describing the displacements and tractions for the underlying fields, the formulation of the linear system whose solution determines the unknown expansion coefficients proceeds in an natural way. The four scalar BCs are satisfied in a pointwise sense, that is, on a specific number of boundary points. According to our previous comments concerning scatterer's geometry, a grid of N equidistantly distributed boundary points consists of the set $\{(r_n,\varphi_n),\ n = 1,\ldots,N\}$, where $r_n = a$, $\varphi_n = 2\pi(n-1)/N$ in the case of a circle and $r_n = h\sqrt{\sinh^2 u_0 + \cos^2 v_n}$, $\varphi_n = \cos^{-1}((h\cosh u_0\cos v_n)/r_n)$, $v_n = 2\pi(n-1)/N$ in the case of an ellipse. An alternative approach exploiting the orthogonality of the trigonometric azimuthal functions is proved to be equivalent due to the employment of the trapezoidal rule in Eqs. (63) and (64). Obviously, in both cases, a truncation procedure needs to be imposed on the infinite series in order for the numerical implementation to become practically feasible. The truncation levels of the infinite series must be in accordance with the selected number of points on the boundary in order to conclude to an algebraic system with equal number of equations and unknowns. Hence, letting L_1 and L_2 denote the levels at which the series in (59) and in (63) and (64) are truncated, respectively, and N the number of points on surface ∂G (either circular or elliptical) at which the set of the four scalar BCs is satisfied, it must hold that $N = L_1 + L_2 + 1$; the choice of these parameters for appropriately solving the resulted linear system is discussed in Section 4.

The final nonhomogeneous system can be written in the matrix form

$$\mathscr{A}\boldsymbol{x} = \boldsymbol{b}, \tag{71}$$

where the $4N\times 4(L_1+L_2+1)$ complex matrix $\mathscr{A}$ is given as

$$\mathscr{A} := \begin{bmatrix} \boldsymbol{\mathscr{B}}_1^{A^{\text{ext}}} & \boldsymbol{\mathscr{B}}_1^{B^{\text{ext}}} & \boldsymbol{\mathscr{D}}_1^{A^+} & \boldsymbol{\mathscr{D}}_1^{A^-} \\ \boldsymbol{\mathscr{B}}_2^{A^{\text{ext}}} & \boldsymbol{\mathscr{B}}_2^{B^{\text{ext}}} & \boldsymbol{\mathscr{D}}_2^{A^+} & \boldsymbol{\mathscr{D}}_2^{A^-} \\ \vdots & \vdots & \vdots & \vdots \\ \boldsymbol{\mathscr{B}}_N^{A^{\text{ext}}} & \boldsymbol{\mathscr{B}}_N^{B^{\text{ext}}} & \boldsymbol{\mathscr{D}}_N^{A^+} & \boldsymbol{\mathscr{D}}_N^{A^-} \end{bmatrix}, \tag{72}$$

with the submatrices $\mathscr{B}_n^s \in \mathbb{C}^{4\times(2L_1+1)}$, $n=1,\ldots,N$, $s=\{A^{\text{ext}},B^{\text{ext}}\}$ and $\mathscr{D}_n^t \in \mathbb{C}^{4\times(2L_2+1)}$, $n=1,\ldots,N$, $t=\{A^+,A^-\}$ defined by

$$\mathscr{B}_n^s := \begin{bmatrix} {}^{(1)}B^s_{-L_1,n} & {}^{(1)}B^s_{-L_1+1,n} & \cdots & {}^{(1)}B^s_{L_1,n} \\ {}^{(2)}B^s_{-L_1,n} & {}^{(2)}B^s_{-L_1+1,n} & \cdots & {}^{(2)}B^s_{L_1,n} \\ {}^{(3)}B^s_{-L_1,n} & {}^{(3)}B^s_{-L_1+1,n} & \cdots & {}^{(3)}B^s_{L_1,n} \\ {}^{(4)}B^s_{-L_1,n} & {}^{(4)}B^s_{-L_1+1,n} & \cdots & {}^{(4)}B^s_{L_1,n} \end{bmatrix}, \tag{73}$$

$$\mathscr{D}_n^t := \begin{bmatrix} {}^{(1)}B^t_{-L_2,n} & {}^{(1)}B^t_{-L_2+1,n} & \cdots & {}^{(1)}B^t_{L_2,n} \\ {}^{(2)}B^t_{-L_2,n} & {}^{(2)}B^t_{-L_2+1,n} & \cdots & {}^{(2)}B^t_{L_2,n} \\ {}^{(3)}B^t_{-L_2,n} & {}^{(3)}B^t_{-L_2+1,n} & \cdots & {}^{(3)}B^t_{L_2,n} \\ {}^{(4)}B^t_{-L_2,n} & {}^{(4)}B^t_{-L_2+1,n} & \cdots & {}^{(4)}B^t_{L_2,n} \end{bmatrix}, \tag{74}$$

and their elements ${}^{(j)}B^s_{m,n}$, $m=-L_1,\ldots,L_1$, $j=1,2,3,4$ and ${}^{(j)}B^t_{m',n}$, $m'=-L_2,\ldots,L_2$, $j=1,2,3,4$ are given in Appendix B. The vector $\boldsymbol{x}$ of the unknown coefficients is defined by

$$\boldsymbol{x} := \left[A^{\text{ext}}_{-L_1} \quad \cdots \quad A^{\text{ext}}_{L_1} \middle| \quad B^{\text{ext}}_{-L_1} \quad \cdots \quad B^{\text{ext}}_{L_1} \middle| \quad A^{+}_{-L_2} \quad \cdots \quad A^{+}_{L_2} \middle| \quad A^{-}_{-L_2} \quad \cdots \quad A^{-}_{L_2} \right]^{\top}, \tag{75}$$

while the right-hand side vector $\boldsymbol{b}$ is given as

$$\boldsymbol{b} := \left[-b_1^{(1)} \quad -b_1^{(2)} \quad -b_1^{(3)} \quad -b_1^{(4)} \middle| \quad \cdots \quad \middle| -b_N^{(1)} \quad -b_N^{(2)} \quad -b_N^{(3)} \quad -b_N^{(4)} \right]^{\top}, \tag{76}$$

with $b_n^{(j)}$, $n=1,\ldots,N$, $j=1,2,3,4$ denoting the projections of the right-hand side of Eq. (65) (resp. Eq. (66)) on $\hat{\boldsymbol{x}}_1$, $\hat{\boldsymbol{x}}_2$ ($j=1,2$) and of Eq. (69) (resp. Eq. (70)) on $\hat{\boldsymbol{x}}_1$, $\hat{\boldsymbol{x}}_2$ ($j=3,4$), calculated at the nth boundary point, in case of longitudinal (resp. transverse) incidence.

The solution of the algebraic linear system (71) leads to the determination of the expansion coefficients for the scattered and the transmitted wave. The far-field representation of the scattered field is obtained by incorporating the large argument representations of the Hankel functions and their derivatives into the expansion (59), which then reads

$$\boldsymbol{u}^{\text{sct}}_{\infty}(\boldsymbol{r}) = \frac{\mathrm{e}^{\mathrm{i}k_{\text{p}}^{\text{ext}}r}}{\sqrt{r}}\boldsymbol{g}_r(\hat{\boldsymbol{r}};\hat{\boldsymbol{d}},\hat{\boldsymbol{p}}) + \frac{\mathrm{e}^{\mathrm{i}k_{\text{s}}^{\text{ext}}r}}{\sqrt{r}}\boldsymbol{g}_{\varphi}(\hat{\boldsymbol{r}};\hat{\boldsymbol{d}},\hat{\boldsymbol{p}}) + \mathrm{O}(r^{-3/2}), \quad |\boldsymbol{r}|\to\infty, \tag{77}$$

with the radial and tangential scattering amplitudes defined over the unit circle be given as

$$\boldsymbol{g}_r(\hat{\boldsymbol{r}};\hat{\boldsymbol{d}},\hat{\boldsymbol{p}}) := \mathrm{i}\left(\frac{2}{\pi k_{\text{p}}^{\text{ext}}}\right)^{1/2} \sum_{m=-L_1}^{L_1} \left\{ A_m^{\text{ext}} \mathrm{e}^{-\mathrm{i}}(2m+1)\frac{\pi}{4}\mathrm{e}^{\mathrm{i}m\varphi} \right\} \hat{\boldsymbol{r}}, \tag{78}$$

$$\boldsymbol{g}_{\varphi}(\hat{\boldsymbol{r}};\hat{\boldsymbol{d}},\hat{\boldsymbol{p}}) := \mathrm{i}\left(\frac{2}{\pi k_{\text{s}}^{\text{ext}}}\right)^{1/2} \sum_{m=-L_1}^{L_1} \left\{ B_m^{\text{ext}} \mathrm{e}^{-\mathrm{i}}(2m+1)\frac{\pi}{4}\mathrm{e}^{\mathrm{i}m\varphi} \right\} (-\hat{\boldsymbol{\varphi}}), \tag{79}$$

and the vector parameters $(\hat{\boldsymbol{r}};\hat{\boldsymbol{d}},\hat{\boldsymbol{p}})$ in the previous definitions corresponding to (observation vector; direction of incidence, polarization vector of incident wave).

4. Numerical results

In this section we present computed results based on the numerical implementation of the semi-analytical scheme described in the previous section. We examine three cases concerning the circular and the

elliptical scatterer as well as the case of a multiple scattering problem involving two circular scatterers each filled with an anisotropic medium exhibiting a specific class of symmetry. The approach to the latter case follows generally the same lines as the one we have already described with only a substantial difference lying in the fact that the scattered field is obtained as the superposition of two outgoing individual fields, each one expressed with respect to a coordinate system associated to each one of the scatterers.

Before presenting results for the aforementioned numerical applications, we give some details about the numerical complexity of the proposed method as well as the checks and comparisons made for validating our solution. The computational load associated with the numerical solution depends both on the length of the truncated expansions, i.e., the parameters L_1, L_2, and the number M of integration points employed by the trapezoidal rule. As far as the selection of M is concerned, it is made on the natural basis that an increase of this parameter does not change the estimated value of the several integrals appreciably (e.g., for $M > 150$, at least 12 significant digits remain unaltered). Needless to say that any other quadrature rule could have been used instead of the trapezoidal one (a Gauss–Legendre quadrature formula has also been employed for comparison purposes). Referring to the truncation levels L_1 and L_2, their values should be generally large since the number $N = L_1 + L_2 + 1$ of 'collocation points', that is, points on the scatterer's surface at which the transmission boundary conditions are enforced, has to be a considerable one in order to obtain a good approximation of the sought-for solution and thus an accurate representation of the involved fields. This fact has, as one might expect, an immediate impact on the condition number of the resulted coefficients matrix $\mathscr{A}$, which can, however, be improved by a normalization of its elements. In particular, the matrix elements ${}^{(j)}B^{A^{\mathrm{ext}}}_{m,n}$, ${}^{(j)}B^{B^{\mathrm{ext}}}_{m,n}$, ${}^{(j)}B^{A^{+}}_{m',n}$ and ${}^{(j)}B^{A^{-}}_{m',n}$ $(j = 1,2,3,4)$ are normalized with $H^{(1)}_m(k_{\mathrm{p}}^{\mathrm{ext}}a)$, $H^{(1)}_m(k_{\mathrm{s}}^{\mathrm{ext}}a)$, $J_{m'}(k_{\mathrm{s}}^{\mathrm{ref}}a)$ and $J_{m'}(k_{\mathrm{p}}^{\mathrm{ref}}a)$, respectively, where $k_{\mathrm{p}}^{\mathrm{ref}}$ and $k_{\mathrm{s}}^{\mathrm{ref}}$ are the wavenumbers of a reference isotropic material and a is a characteristic dimension of the scatterer under consideration. The aforementioned material with the dimensionless values $\lambda_{\mathrm{ref}} = 2.0$ and $\mu_{\mathrm{ref}} = 1.5$ for the Lamé constants and the dimensionless mass density $\rho_{\mathrm{ref}} = 2.0$, will serve in the sequel as a standard one wherever scattering by an isotropic inclusion is encountered. Following this procedure and solving the system of Eq. (71) by an LU decomposition algorithm for the normalized nonsymmetric square matrix $\mathscr{A}$, at least four-digit convergence has been achieved in all cases with truncation numbers $18 \leqslant L_1 = L_2 \leqslant 20$.

The numerical calculations were checked in several ways. Energy consistency has been checked by application of the well-known forward-scattering theorem (Dassios et al., 1995), which states that

$$\sigma_{\mathrm{p}} = 2\sqrt{\frac{\pi}{k_{\mathrm{p}}^{\mathrm{ext}}}}\mathrm{Im}\{(1-\mathrm{i})g_r(\hat{\boldsymbol{d}};\hat{\boldsymbol{d}},\hat{\boldsymbol{d}})\}, \tag{80}$$

$$\sigma_{\mathrm{s}} = 2\sqrt{\frac{\pi}{k_{\mathrm{s}}^{\mathrm{ext}}}}\mathrm{Im}\{(1-\mathrm{i})g_\varphi(\hat{\boldsymbol{d}};\hat{\boldsymbol{d}},\hat{\boldsymbol{\varphi}}_{\boldsymbol{d}})\}, \tag{81}$$

where the polarization vector $\hat{\boldsymbol{\varphi}}_{\boldsymbol{d}}$ is obtained by rotating $\hat{\boldsymbol{d}}$ anticlockwise by $\pi/2$ and the total scattering cross-sections σ_{p} and σ_{s} for plane wave P- or S-incidence (see Eqs. (65) and (66)), respectively, are defined by

$$\sigma_{\mathrm{p}} := k_{\mathrm{p}}^{\mathrm{ext}}\int_0^{2\pi}\left\{(k_{\mathrm{p}}^{\mathrm{ext}})^{-1}|g_r(\hat{\boldsymbol{r}};\hat{\boldsymbol{d}},\hat{\boldsymbol{d}})|^2 + (k_{\mathrm{s}}^{\mathrm{ext}})^{-1}|g_\varphi(\hat{\boldsymbol{r}};\hat{\boldsymbol{d}},\hat{\boldsymbol{d}})|^2\right\}\mathrm{d}\varphi, \tag{82}$$

$$\sigma_{\mathrm{s}} := k_{\mathrm{s}}^{\mathrm{ext}}\int_0^{2\pi}\left\{(k_{\mathrm{p}}^{\mathrm{ext}})^{-1}|g_r(\hat{\boldsymbol{r}};\hat{\boldsymbol{d}},\hat{\boldsymbol{\varphi}}_{\boldsymbol{d}})|^2 + (k_{\mathrm{s}}^{\mathrm{ext}})^{-1}|g_\varphi(\hat{\boldsymbol{r}};\hat{\boldsymbol{d}},\hat{\boldsymbol{\varphi}}_{\boldsymbol{d}})|^2\right\}\mathrm{d}\varphi. \tag{83}$$

The relative error computed by independent calculations of each side of (80) and (81) was generally less than 0.05%. Moreover, our solution has successfully passed the test of conforming with the principle of reciprocity, which in the present case is expressed through the relations

$$g_r(\hat{\boldsymbol{r}};\hat{\boldsymbol{d}},\hat{\boldsymbol{d}}) = g_r(-\hat{\boldsymbol{d}};-\hat{\boldsymbol{r}},-\hat{\boldsymbol{r}}), \tag{84}$$

$$g_r(\hat{\boldsymbol{r}};\hat{\boldsymbol{d}},\hat{\boldsymbol{\varphi}}_{\boldsymbol{d}}) = (k_{\mathrm{p}}^{\mathrm{ext}}/k_{\mathrm{s}}^{\mathrm{ext}})^{3/2} g_{\varphi}(-\hat{\boldsymbol{d}};-\hat{\boldsymbol{r}},-\hat{\boldsymbol{r}}), \tag{85}$$

$$g_{\varphi}(\hat{\boldsymbol{r}};\hat{\boldsymbol{d}},\hat{\boldsymbol{d}}) = (k_{\mathrm{s}}^{\mathrm{ext}}/k_{\mathrm{p}}^{\mathrm{ext}})^{3/2} g_r(-\hat{\boldsymbol{d}};-\hat{\boldsymbol{r}},-\hat{\boldsymbol{\varphi}}), \tag{86}$$

$$g_{\varphi}(\hat{\boldsymbol{r}};\hat{\boldsymbol{d}},\hat{\boldsymbol{\varphi}}_{\boldsymbol{d}}) = g_{\varphi}(-\hat{\boldsymbol{d}};-\hat{\boldsymbol{r}},-\hat{\boldsymbol{\varphi}}). \tag{87}$$

Furthermore, the results obtained by the proposed method have been tested against those produced by other methods for some particular cases. At a first stage, a comparison has been made with the outcomes of a pure analytic solution derived by the authors to the problem of scattering of plane waves from an isotropic circular inclusion, which is based on the employment of Bessel–Fourier expansions for the elastic field in the interior of the scatterer. The comparison has lead to an excellent agreement verifying simultaneously the accuracy of the numerical evaluation of the basic functions $\Phi_m^{\pm}$ and $\Theta_m^{\pm}$ used in the present study. At a next stage, our solution is compared with existing computational results provided by a BEM approach (Polyzos et al., 1998; Verbis et al., 2001) to the scattering problem of plane waves by an isotropic inclusion. For the shake of brevity, comparison is herein restricted to the indicative case depicted in Fig. 1, which corresponds to the scattering of a P-incident plane wave propagating at an angle $\alpha = 0$, by an isotropic elliptical inclusion with semi-axes ratio equal to 1.2 and elastic parameters equal to those of the reference material mentioned above. The Poisson ratio for the isotropic background medium has been taken equal to 0.25 and the dimensionless frequency $k_{\mathrm{p}}^{\mathrm{ext}} a_0 = 1.0$, with a_0 being the major semi-axis of the elliptical cross-section. As it is apparent, the agreement between the two methods is excellent.

We now proceed with the numerical applications described at the beginning of the section, which all deal with a special case of an orthotropic medium, namely a cubic medium with three independent stiffness coefficients since cubic symmetry class establishes the additional symmetry relation $C_{2222} = C_{1111}$ or equivalently $Q_{22} = Q_{11}$ between the stiffness matrix elements. For the isotropic host medium we assume the dimensionless values $\lambda = \mu = 1.0$ for the Lamé constants and the dimensionless density $\rho_{\mathrm{ext}} = 1.0$. It is mentioned that the assumption of equal Lamé constants is by no means an essential or a restrictive one, but it

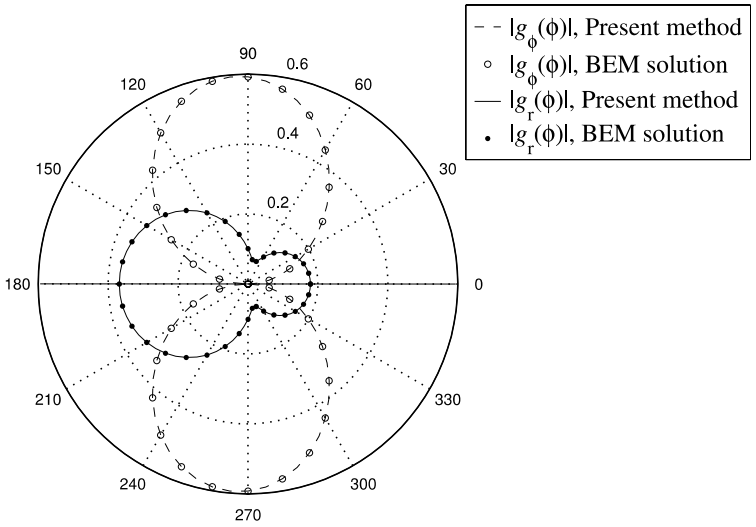

Fig. 1. Angular distribution of the scattering amplitudes $|g_r(\varphi)|$ and $|g_{\varphi}(\varphi)|$ for P-incidence with $\alpha = 0$ on an isotropic elliptical inclusion.

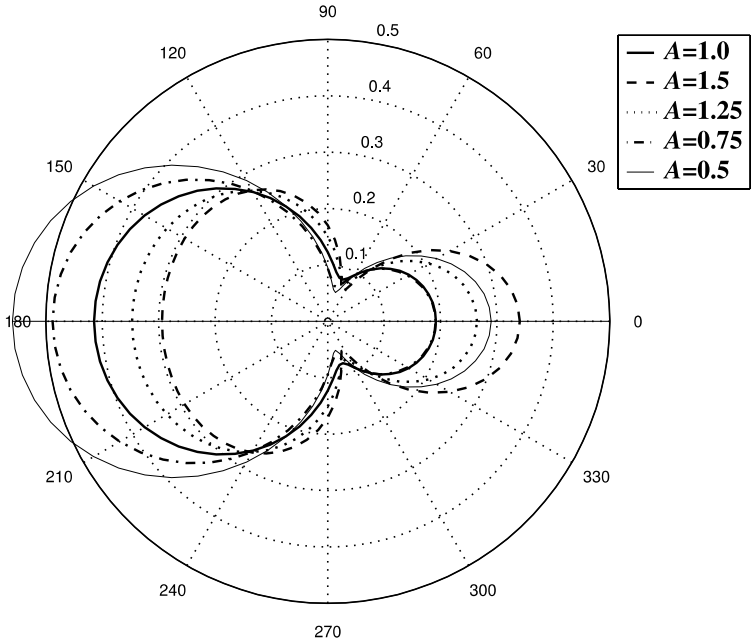

Fig. 2. Angular distribution of the radial scattering amplitude $|g_r(\varphi)|$ for P-incidence with $\alpha = 0$ on the circular inclusion.

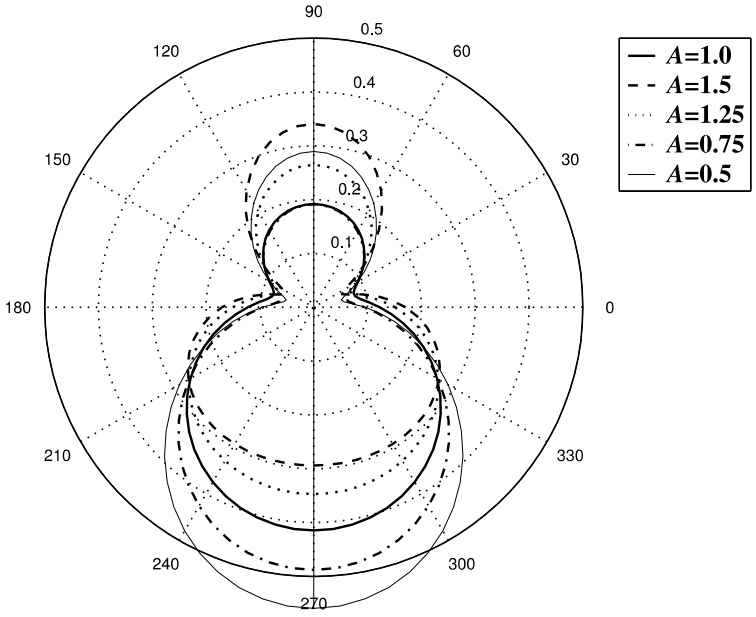

Fig. 3. Angular distribution of the radial scattering amplitude $|g_r(\varphi)|$ for P-incidence with $\alpha = \pi/2$ on the circular inclusion.

serves our primary objective of focusing only on the properties of the anisotropic inclusion. For the cubic material, the density is $\rho_{\text{int}} = 2.0$ and $k_{\text{p}}^{\text{ext}} a = 1.0$ is the dimensionless frequency, where a is the radius of the

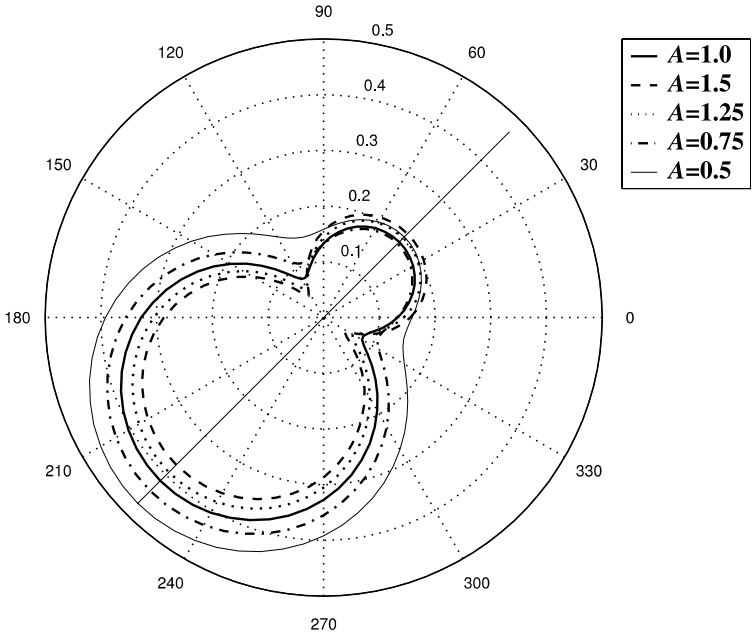

Fig. 4. Angular distribution of the radial scattering amplitude $|g_r(\varphi)|$ for P-incidence with $\alpha = \pi/4$ on the circular inclusion.

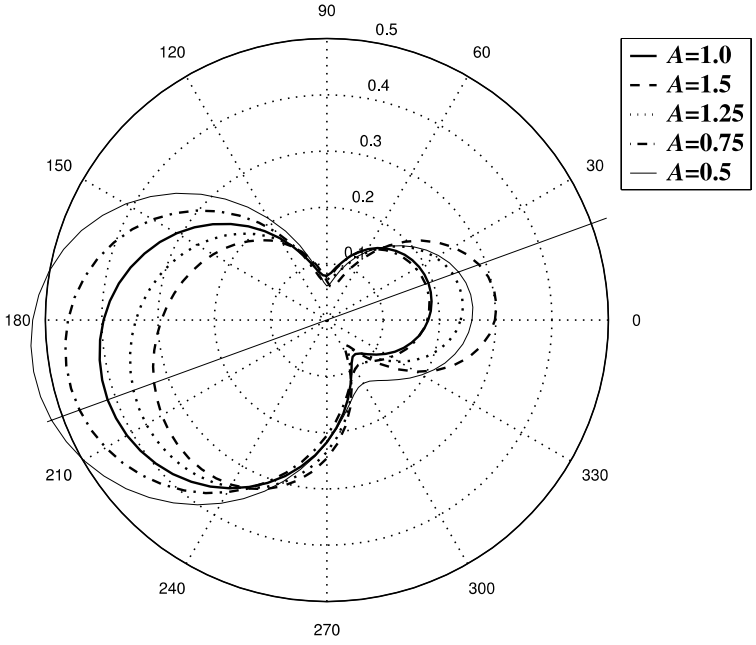

Fig. 5. Angular distribution of the radial scattering amplitude $|g_r(\varphi)|$ for P-incidence with $\alpha = \pi/9$ on the circular inclusion.

circular cross-section or the major semi-axis of the elliptical one. In addition, we introduce the cubic anisotropy ratio, which is also referred to as Zener anisotropy factor

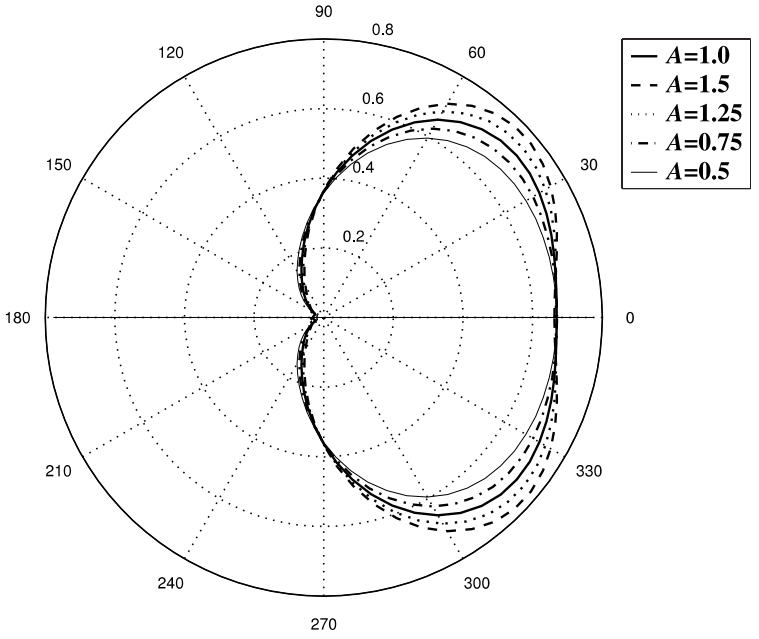

Fig. 6. Angular distribution of the tangential scattering amplitude $|g_{\varphi}(\varphi)|$ for S-incidence with $\alpha = 0$ on the circular inclusion.

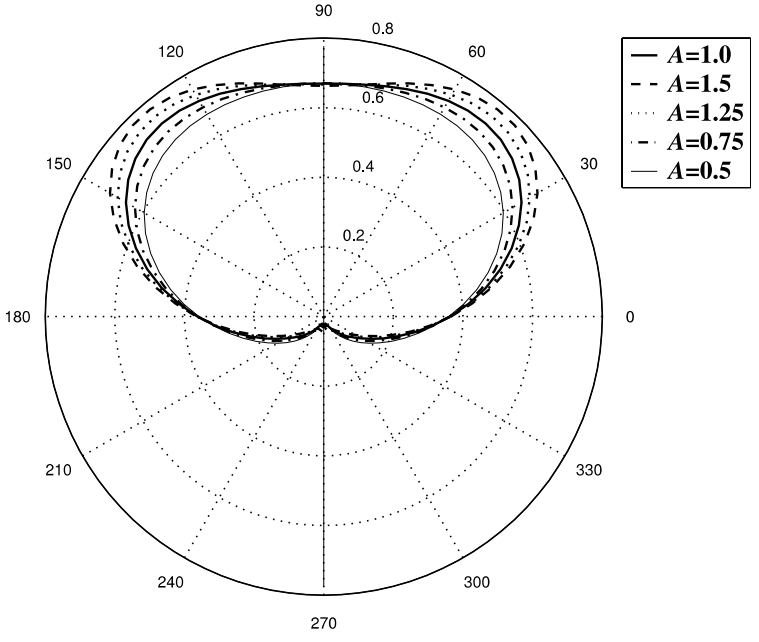

Fig. 7. Angular distribution of the tangential scattering amplitude $|g_{\varphi}(\varphi)|$ for S-incidence with $\alpha = \pi/2$ on the circular inclusion.

$$A := \frac{2Q_{66}}{Q_{11} - Q_{12}}, \tag{88}$$

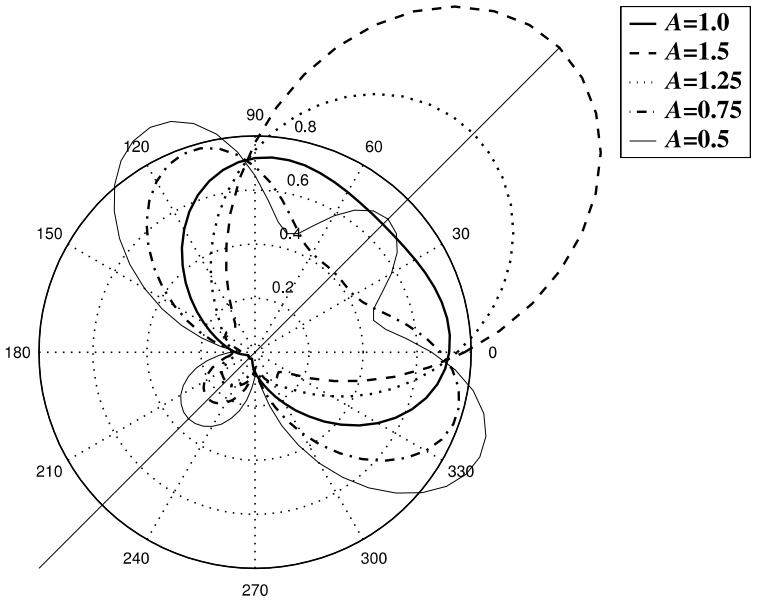

Fig. 8. Angular distribution of the tangential scattering amplitude $|g_\varphi(\varphi)|$ for S-incidence with $\alpha = \pi/4$ on the circular inclusion.

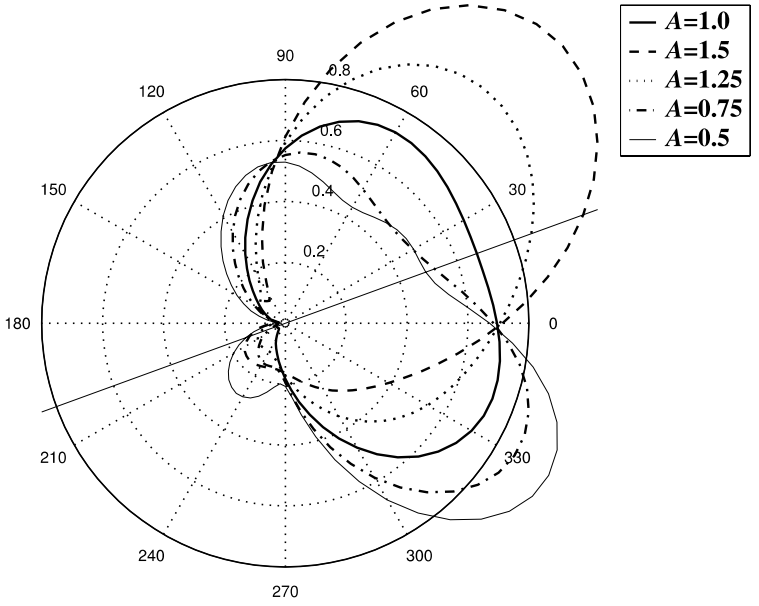

Fig. 9. Angular distribution of the tangential scattering amplitude $|g_\varphi(\varphi)|$ for S-incidence with $\alpha = \pi/9$ on the circular inclusion.

with the degree of anisotropy measured by the deviation of A from the value $A = 1.0$, valid for an isotropic medium. In the forthcoming examples, the case $A = 1.0$ always corresponds to the reference isotropic material. Moreover, the relative deviation of a quantity u, say, from the isotropic case is defined by

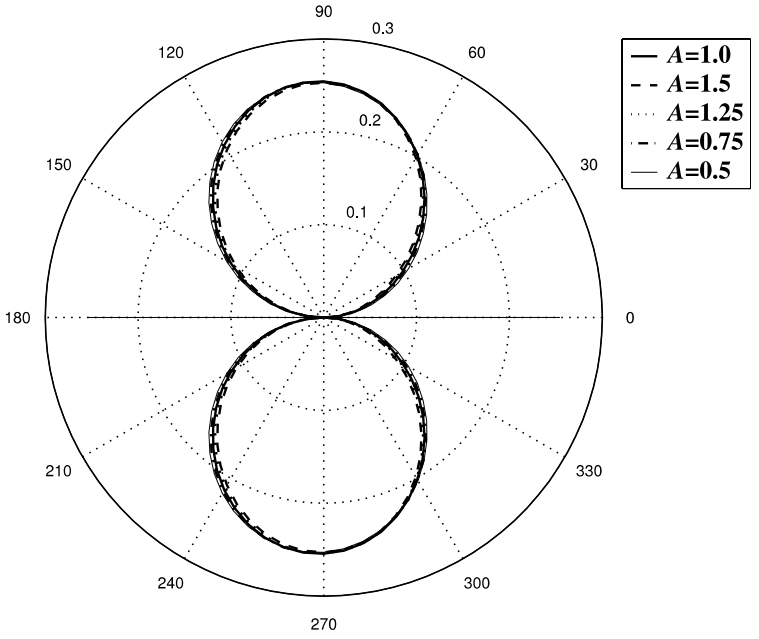

Fig. 10. Angular distribution of the radial scattering amplitude $|g_r(\varphi)|$ for S-incidence with $\alpha = 0$ on the circular inclusion.

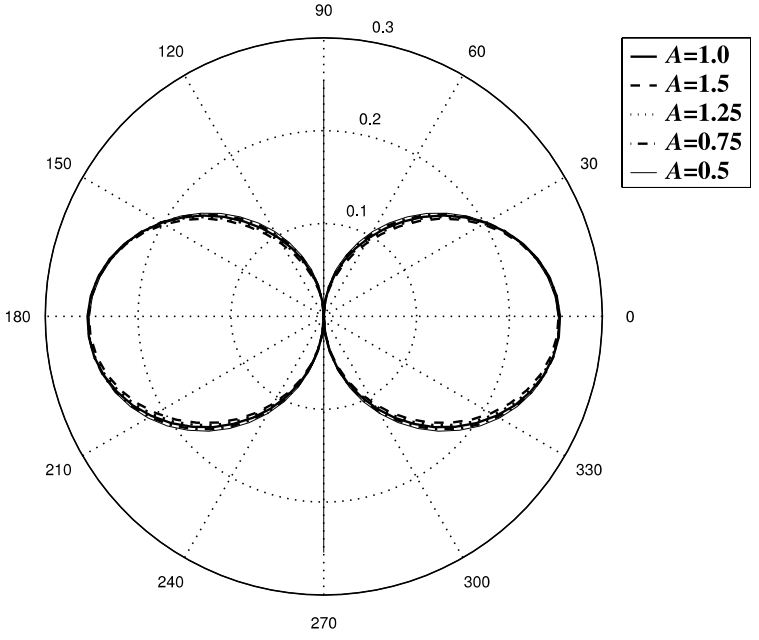

Fig. 11. Angular distribution of the radial scattering amplitude $|g_r(\varphi)|$ for S-incidence with $\alpha = \pi/2$ on the circular inclusion.

$$\mathrm{RD}(u) := \frac{u_{|A\neq 1} - u_{|A=1}}{u_{|A=1}} = \frac{u_{|\text{anisotropy}} - u_{|\text{isotropy}}}{u_{|\text{isotropy}}}. \tag{89}$$

Finally, we select angles of incidence in the range of 0 to $\pi/2$, including $\pi/4$, which coincides with a symmetry plane of the cubic material. We remind that the cubic material in the 2D-case has four planes of symmetry whose normals are on the coordinate axes and on the coordinate planes making an angle $\pi/4$ with the coordinate axes.

Figs. 2–15 correspond to the case where the elastic inclusion is one of circular cross-section. In Figs. 2–5, the angular distribution of the radial scattering amplitude $|g_r(\varphi)|$ is shown for several angles of longitudinal P-incidence α and varying anisotropy factor A. In the case of $\alpha = 0$ the effect of the anisotropy is pronounced in both the forward and backscattering direction for any value of A. We also observe that the distributions are symmetric with respect to the direction of incidence since the latter coincides with a plane of material symmetry. The same observations hold for $\alpha = \pi/2$, which is also a plane of symmetry and furthermore, a comparison with the previous example verifies that the cubic structure preserves its symmetry properties under $\pi/2$ rotations about x_1-axis. For $\pi/4$ incidence, the symmetry is also preserved but the effect of the anisotropy on the computed quantities is weaker, especially in the forward scattering direction, for any value of A. Finally, for an angle of incidence which does not coincide with a plane of symmetry, e.g., $\pi/9$, the symmetry w.r.t. the direction of incidence is no longer preserved except, of course, when $A = 1.0$ corresponding to isotropy.

In Figs. 6–9, the magnitude of the tangential scattering amplitude $|g_\varphi(\varphi)|$ for transverse S-incidence at several angles is examined. In this case, $\alpha = 0$ and $\pi/2$ have almost no effect on the computed quantity for any value of the anisotropy factor. In contrast, a $\pi/4$ incidence is shown to be the one that reveals the anisotropy and up to a point its measure. Our previous remarks relatively to the symmetry of the distributions w.r.t. the angle of incidence are also valid here as one may observe from the case of $\pi/9$ incidence.

We proceed with the examination of a 'mixed' case, in the sense that the incidence is of the transverse type, i.e., an S-wave, and the radial scattering amplitude $|g_r(\varphi)|$ is observed. Figs. 10–13 correspond to this case. The first plot referring to $\alpha = 0$ actually demonstrates that such a combination of incidence-observation is unsuitable for detecting the presence of the anisotropy. The same holds for $\alpha = \pi/2$, while in the case of $\alpha = \pi/4$ the effect of the anisotropy, as far as the magnitudes of the computed quantities are concerned, is

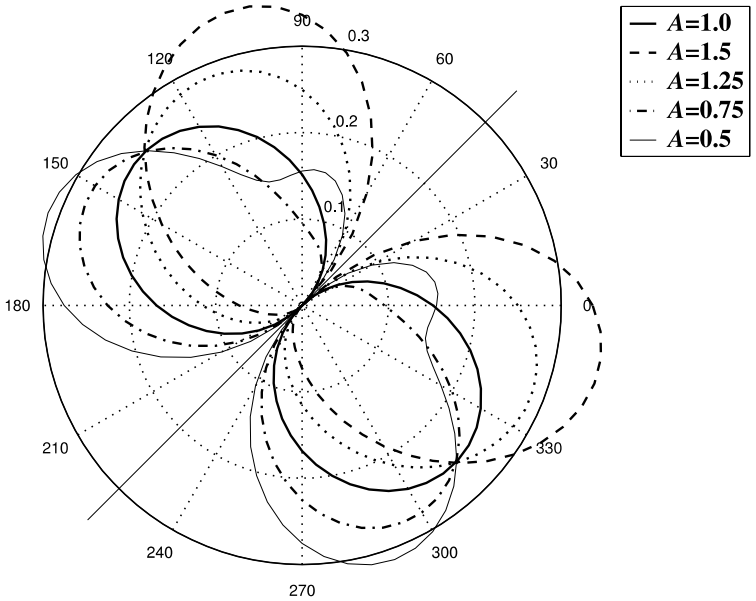

Fig. 12. Angular distribution of the radial scattering amplitude $|g_r(\varphi)|$ for S-incidence with $\alpha = \pi/4$ on the circular inclusion.

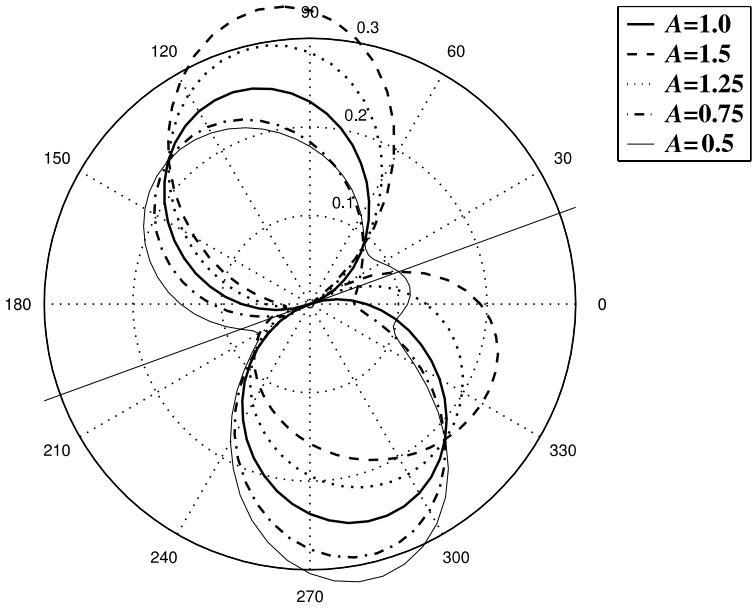

Fig. 13. Angular distribution of the radial scattering amplitude $|g_r(\varphi)|$ for S-incidence with $\alpha = \pi/9$ on the circular inclusion.

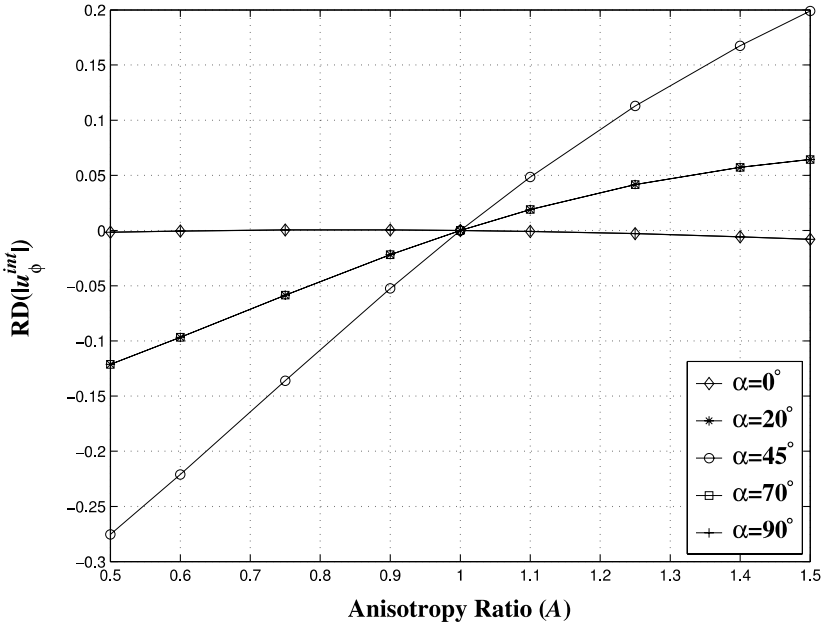

Fig. 14. Relative deviation of the tangential displacement $|u_{\varphi}^{\mathrm{int}}|$ on the circular boundary versus anisotropy factor (A) for S-incidences and $\varphi = \alpha$.

certainly smaller compared with the corresponding case where the tangential scattering amplitude was observed, i.e., Fig. 8. The loss of symmetry is again obvious for an incidence of $\pi/9$.

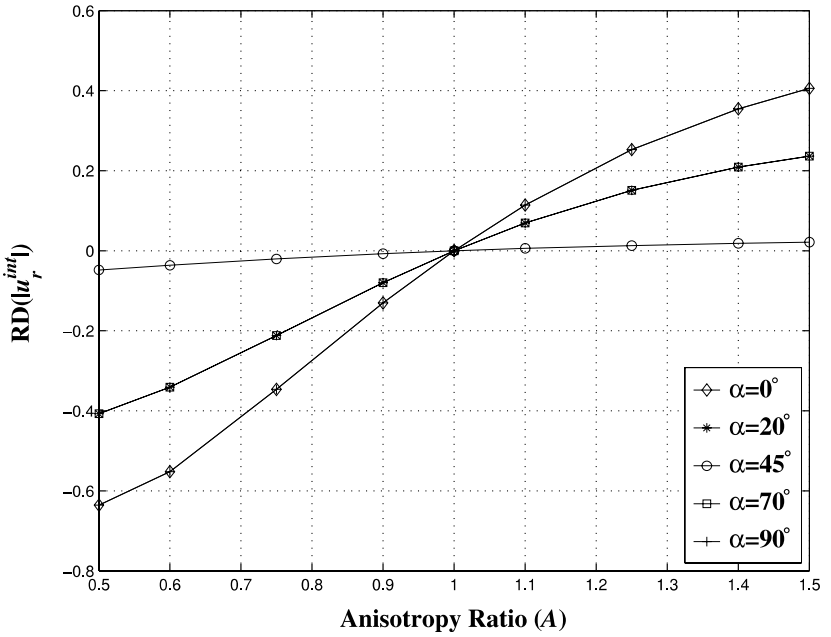

Fig. 15. Relative deviation of the radial displacement $|u_r^{\text{int}}|$ on the circular boundary versus anisotropy factor (A) for P-incidences and $\varphi = \pi + \alpha$.

The previous results clearly indicate that the information on the specific anisotropic character of the anisotropic inclusion is encoded in the far-field scattered wave. In the sequel we present computed results concerning boundary values of the transmitted field. In Fig. 14, we examine the relative deviation from the isotropic case of the circumferential component of the interior displacement field computed on the circular boundary versus the anisotropy factor for transverse incidences and for an observation direction which coincides with the incident one. We first notice that the results are in complete agreement with the corresponding case where the far-field quantity, i.e., the tangential scattering amplitude was observed (see Figs. 6–9). Indeed, the $\pi/4$ incidence causes the greatest deviation from the isotropic case, while for $\alpha = 0$ and $\pi/2$ the relative deviation tends to zero for any value of A. We also observe that the sign of the computed ratio follows a specific rule depending on the value of A being greater or less than 1.0. For completeness, the case of P-type incidences and observation of the radial displacement in a direction being opposite to the incident one is shown in Fig. 15, where now 0 and $\pi/2$ incidences cause the greatest deviation from the isotropic case and the sign of RD follows the same rule. The agreement with the results presented in Figs. 2–5 is again obvious.

Numerical results referring to the case of an elastic inclusion of elliptical cross-section with semi-axes ratio equal to 1.2 are shown in Figs. 16–20. They are in quantitative agreement with those concerning the circular scatterer as one may observe by comparing Figs. 16–19 with Figs. 6–9 with a qualitative difference lying in the fact that the distributions are no longer expected to be symmetric w.r.t. the direction of incidence when $\alpha = \pi/4$. Fig. 20 confirms once more the consistency of the results obtained upon observing far-field and near-field quantities.

Finally, we consider a multiple scattering problem involving two circular scatterers each filled with the same cubic anisotropic medium. The inclusions are of equal cross-sections with their centers located at the points $(\lambda_p, 0)$ and $(-\lambda_p, 0)$ on the x_1-axis, where λ_p is the wavelength of the longitudinal wave in

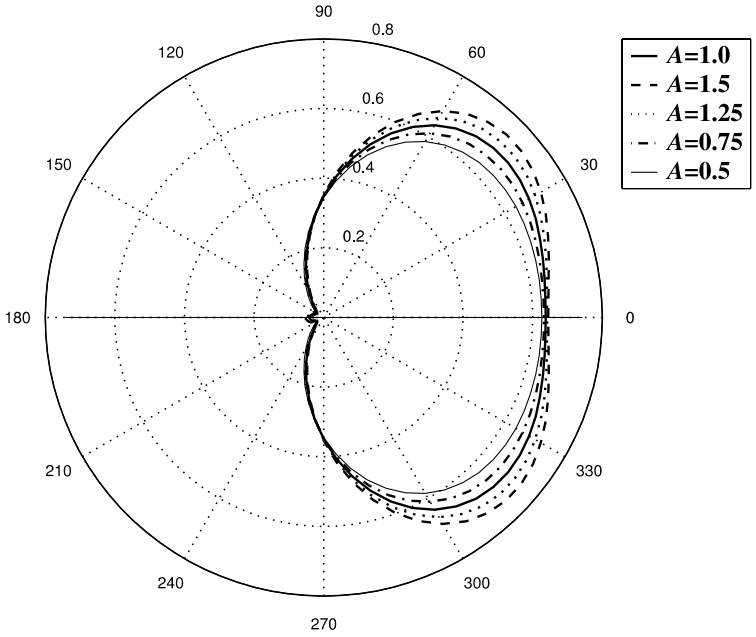

Fig. 16. Angular distribution of the tangential scattering amplitude $|g_{\varphi}(\varphi)|$ for S-incidence with $\alpha = 0$ on the elliptical inclusion.

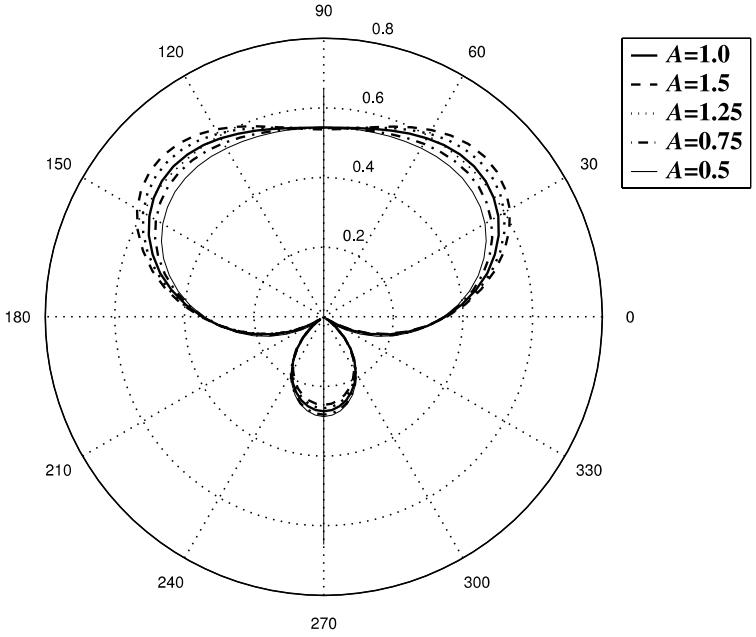

Fig. 17. Angular distribution of the tangential scattering amplitude $|g_{\varphi}(\varphi)|$ for S-incidence with $\alpha = \pi/2$ on the elliptical inclusion.

the background medium. In Figs. 21 and 22 the relative deviation from isotropy of the circumferential component of the field transmitted in the right and the left inclusion, respectively, is shown. The observation

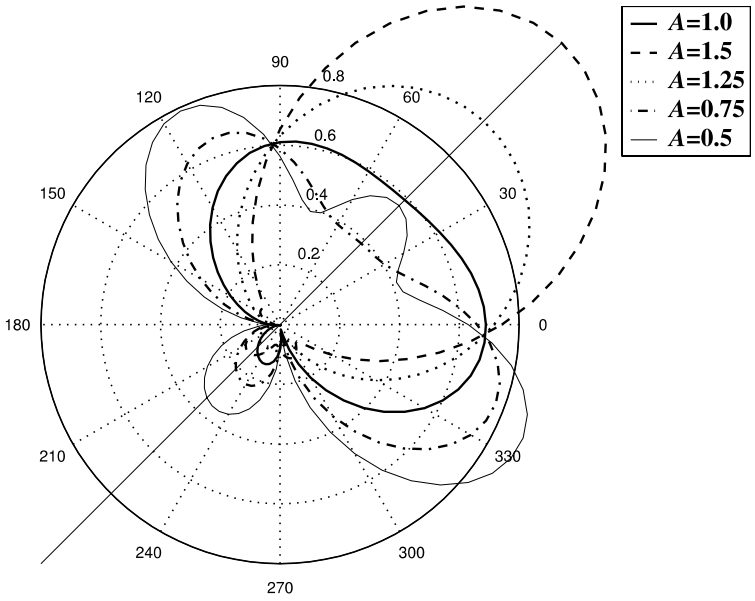

Fig. 18. Angular distribution of the tangential scattering amplitude $|g_\varphi(\varphi)|$ for S-incidence with $\alpha = \pi/4$ on the elliptical inclusion.

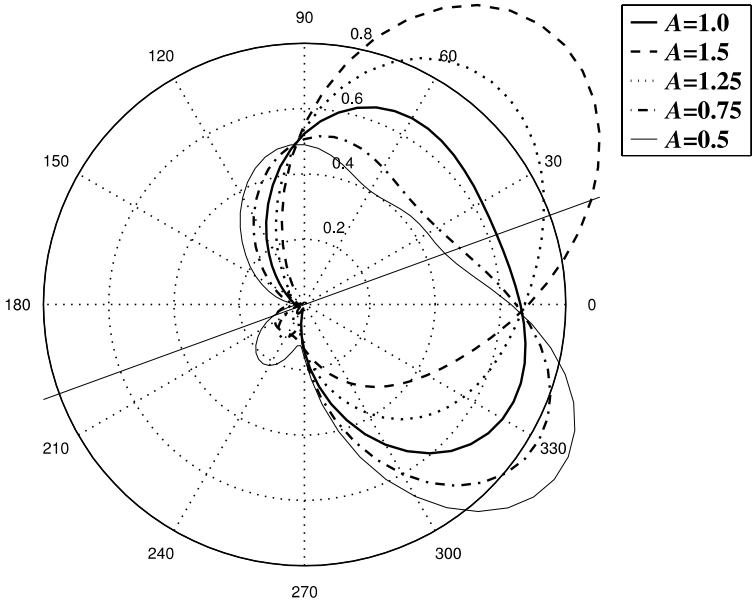

Fig. 19. Angular distribution of the tangential scattering amplitude $|g_\varphi(\varphi)|$ for S-incidence with $\alpha = \pi/9$ on the elliptical inclusion.

direction of the transmitted fields coincides with the incident one and therefore a comparison with Fig. 14, where the corresponding case of a single circular inclusion is considered, can be made. The similarity between the obtained results in the two cases is obvious.

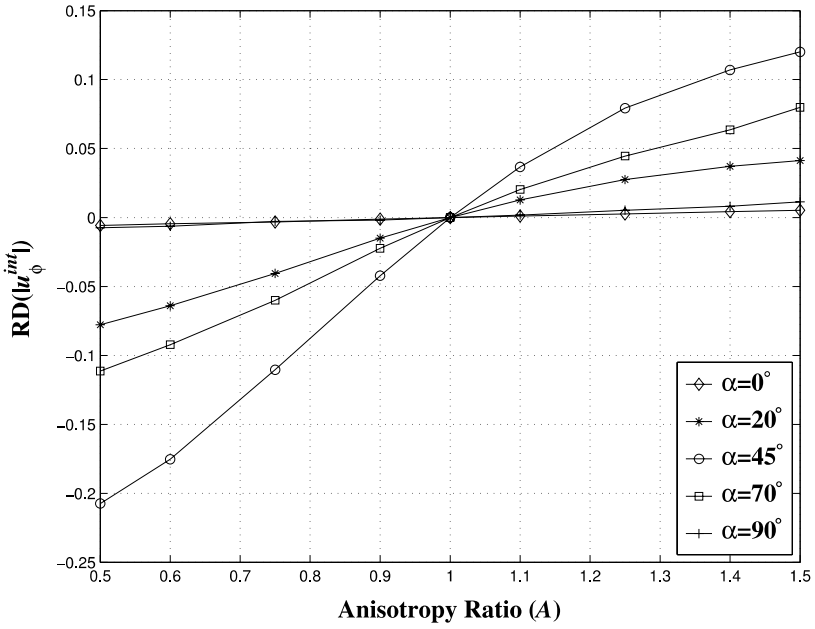

Fig. 20. Relative deviation of the tangential displacement $|u_{\varphi}^{\mathrm{int}}|$ on the elliptical boundary versus anisotropy factor (A) for S-incidences and $\varphi = \pi + \alpha$.

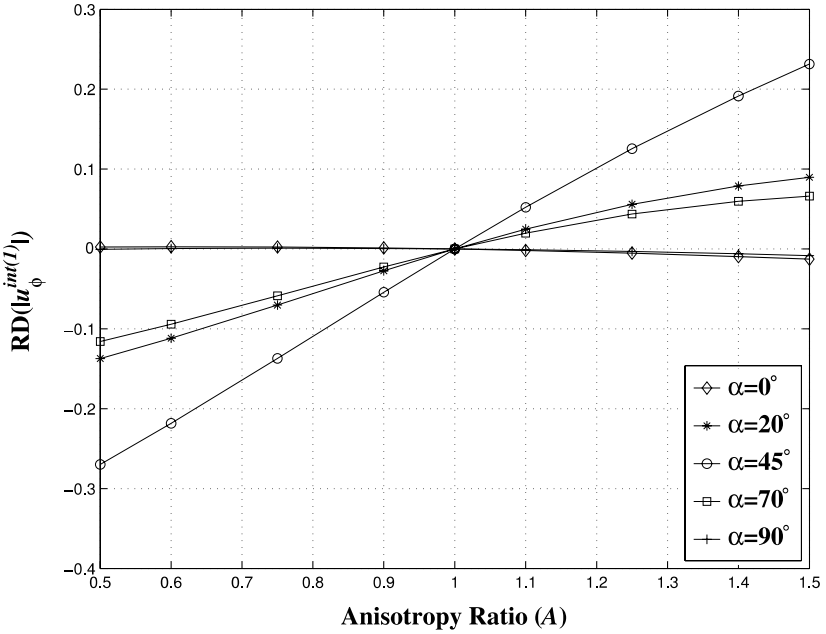

Fig. 21. Relative deviation of the tangential displacement $|u_{\varphi}^{\mathrm{int}(1)}|$ on the boundary of the right circular inclusion versus anisotropy factor (A) for S-incidences and $\varphi = \alpha$.

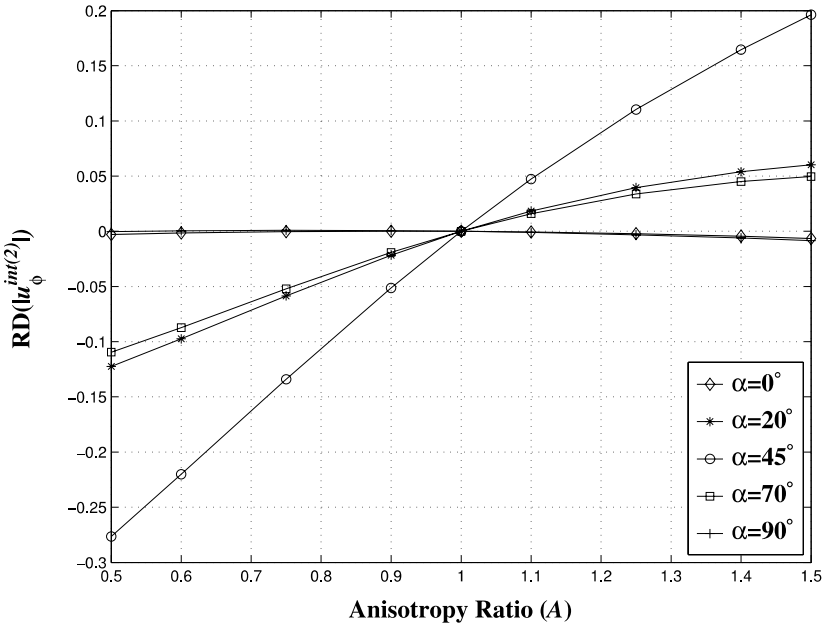

Fig. 22. Relative deviation of the tangential displacement $|u_{\varphi}^{\mathrm{int}(2)}|$ on the boundary of the left circular inclusion versus anisotropy factor (A) for S-incidences and $\varphi = \alpha$.

5. Conclusions

The problem of a rigorous analysis of the elasticity equations governing the elastic behavior of an orthotropic material in two dimensions was addressed in this paper. This analysis resulted in a Fourier series expansion for the displacement field describing the elastic deformations of the orthotropic medium. A mathematical model for the solution of the associated transmission scattering problem, taking advantage of the aforementioned expansion was also settled. Numerical results for an inclusion of circular or elliptical cross-section as well as for two circular inclusions with material properties characterized by the cubic symmetry class-a special case of the orthotropic class of symmetry-were presented. These examples have revealed the possibility of recovering the special features of the scatterer's anisotropic behavior based on an appropriate interpretation of the observation results referring to either far-field or near-field quantities for suitably chosen types and angles of incidence.

Appendix A

We briefly discuss the arguments leading to the establishment of the denseness of the function set $\mathcal{Q}$ defined in Eq. (42) in the space of solutions of equation $L\Psi = 0$, where L is the operator defined in Eq. (26). We first of all define

$$\mathcal{W}(G) = \{v \in C^4(G) \cap C^3(\overline{G}) : \ Lv = 0 \text{ in } G\}, \tag{90}$$

and denote by $\overline{\mathcal{W}(G)}$ the $H^2(G)$ closure of $\mathcal{W}(G)$. We then consider the integral operator $H : \ [L^2(0, 2\pi)]^2 \to \overline{\mathcal{W}(G)}$ defined by

$$(HA)(\boldsymbol{r}) = \int_0^{2\pi} [A_+(u)\mathrm{e}^{-\mathrm{i}k_+(u)\hat{\boldsymbol{k}}\cdot\boldsymbol{r}}]\,\mathrm{d}u + \int_0^{2\pi} [A_-(u)\mathrm{e}^{-\mathrm{i}k_-(u)\hat{\boldsymbol{k}}\cdot\boldsymbol{r}}]\,\mathrm{d}u, \tag{91}$$

where $A := (A_+, A_-) \in [L^2(0,2\pi)]^2$. It is obvious that as the functions $A(u)$ run over $[L^2(0,2\pi)]^2$, the functions $(HA)(\boldsymbol{r})$ 'build' the space $\mathscr{Q}$.

Our primary objective is to show that the $H^2(G)$ closure of $\mathscr{Q}$ coincides with $\overline{\mathscr{W}(G)}$. To this end, we will first examine the denseness properties of the traces of functions belonging to the aforementioned spaces. More precisely, the classical trace theory for Sobolev spaces (Wloka, 1987) ensures that every function v belonging to $\overline{\mathscr{W}(G)} \subset H^2(G)$ disposes interior traces $\gamma_0^- v \in H^{3/2}(\partial G)$ and $\gamma_1^- v \in H^{1/2}(\partial G)$ (here and in the sequel, by the superscripts $(+)$ and $(-)$ we distinguish the limits obtained by approaching the boundary ∂G from $\mathbb{R}^2 \setminus \overline{G}$ and G, respectively). If the function v is smooth enough for its boundary values to exist in the classical sense, then one simply has $\gamma_0^- v \equiv v|_{\partial G}$ and $\gamma_1^- v \equiv \frac{\partial v}{\partial \nu}\big|_{\partial G}$. It is sufficient for our purposes to show that the space $\mathscr{R} := \gamma_0^- \mathscr{Q} \times \gamma_1^- \mathscr{Q}$ is dense in the product space $X := H^{3/2}(\partial G) \times H^{1/2}(\partial G)$, since then the application of continuity arguments in boundary value problems 'transfers' this property to the interior space as well. With this in mind, we first note that establishing the required denseness property $\overline{\mathscr{R}} = X$ is equivalent to showing that $\mathscr{R}^a = \{0\}$, where $\mathscr{R}^a$ is the annihilator set of $\mathscr{R}$ (McLean, 2000) defined as the closed subspace of the dual space $X^* := H^{-3/2}(\partial G) \times H^{-1/2}(\partial G)$ consisting of all the functionals that annihilate $\mathscr{R}$. In particular, if $(h, f) \in \mathscr{R}^a$ then one has to show that the relation

$$\left\langle (h,f), \left(HA, \frac{\partial}{\partial \nu}(HA)\right)\right\rangle_{X^*\times X} := \int_{\partial G} h(\boldsymbol{r})(HA)(\boldsymbol{r})\,\mathrm{d}s(\boldsymbol{r}) + \int_{\partial G} f(\boldsymbol{r})\frac{\partial}{\partial \nu}(HA)(\boldsymbol{r})\,\mathrm{d}s(\boldsymbol{r}) = 0, \tag{92}$$

for every $A \in [L^2(0,2\pi)]^2$ implies that $h = f = 0$, where $\langle\cdot,\cdot\rangle_{X^*\times X}$ denotes the corresponding duality pairing. Hence, assuming that relation (92) holds, we introduce representation (91) in (92) and interchange the order of integration to obtain that

$$\sum_{\pm} \int_0^{2\pi} A_\pm(u)\left\{\int_{\partial G}\left[\mathrm{e}^{-\mathrm{i}k_\pm(u)\hat{\boldsymbol{k}}\cdot\boldsymbol{r}} h(\boldsymbol{r}) + \frac{\partial}{\partial \nu(\boldsymbol{r})}(\mathrm{e}^{-\mathrm{i}k_\pm(u)\hat{\boldsymbol{k}}\cdot\boldsymbol{r}}) f(\boldsymbol{r})\right]\mathrm{d}s(\boldsymbol{r})\right\}\mathrm{d}u = 0, \tag{93}$$

for every $(A_+, A-) \in [L^2(0,2\pi)]^2$. Consequently, upon defining

$$\mathscr{H}_\pm(u) := \int_{\partial G} \mathrm{e}^{-\mathrm{i}k_\pm(u)\hat{\boldsymbol{k}}\cdot\boldsymbol{r}} h(\boldsymbol{r})\,\mathrm{d}s(\boldsymbol{r}) + \int_{\partial G} \frac{\partial}{\partial \nu(\boldsymbol{r})}(\mathrm{e}^{-\mathrm{i}k_\pm(u)\hat{\boldsymbol{k}}\cdot\boldsymbol{r}}) f(\boldsymbol{r})\,\mathrm{d}s(\boldsymbol{r}), \tag{94}$$

we have that $\mathscr{H}_\pm(u) = 0$ for every $u \in [0,2\pi)$. With the intention to identify $\mathscr{H}_\pm(u)$, $u \in [0,2\pi)$ as the asymptotic form of a radiating field belonging to $\operatorname{Ker} L$, we proceed by showing that the trigonometric exponential kernels appearing in the integrals of the definition (94) are closely related to the asymptotic formula for the Green's function associated with the operator L.

In particular, the Green's function $\Gamma(\boldsymbol{r}, \boldsymbol{r}')$ has the integral representation

$$\Gamma(\boldsymbol{r},\boldsymbol{r}') = \frac{1}{(2\pi)^2}\int_{\mathbb{R}^2} \mathrm{d}\boldsymbol{k}\frac{\mathrm{e}^{\mathrm{i}\boldsymbol{k}\cdot(\boldsymbol{r}-\boldsymbol{r}')}}{L(\mathrm{i}k_1, \mathrm{i}k_2)} = \frac{1}{4}\frac{1}{(2\pi)^2}\int_0^{2\pi}\frac{\mathrm{d}u}{D_2(u)}\int_0^\infty \mathrm{d}k\frac{k\mathrm{e}^{\mathrm{i}\boldsymbol{k}\cdot(\boldsymbol{r}-\boldsymbol{r}')}}{[k^2 - k_+^2(u)][k^2 - k_-^2(u)]}. \tag{95}$$

The evaluation of the integral on the real positive semi-axis is accomplished via an appropriate complex integration technique taking into account the outgoing radiating behavior of the Green's function. Following this procedure, we finally arrive at the following expression:

$$\begin{aligned}\Gamma(\boldsymbol{r},\boldsymbol{r}') = {} & \frac{1}{4}\frac{\mathrm{i}}{(2\sqrt{\pi})^2}\int_{\gamma-\pi/2}^{\gamma+\pi/2}\frac{\mathrm{d}u}{\rho\omega^2\sqrt{D_1(u)}}\left[\mathrm{e}^{\mathrm{i}k_+(u)\hat{\boldsymbol{k}}\cdot(\boldsymbol{r}-\boldsymbol{r}')} - \mathrm{e}^{\mathrm{i}k_-(u)\hat{\boldsymbol{k}}\cdot(\boldsymbol{r}-\boldsymbol{r}')}\right] \\ & + \frac{1}{4}\frac{1}{(2\pi)^2}\int_0^{2\pi}\frac{\mathrm{d}u}{\rho\omega^2\sqrt{D_1(u)}}[g(k_+(u)|q|) - g(k_-(u)|q|)],\end{aligned} \tag{96}$$

where $\boldsymbol{r}-\boldsymbol{r}'=|\boldsymbol{r}-\boldsymbol{r}'|(\cos\gamma,\sin\gamma)$, $q=\hat{\boldsymbol{k}}\cdot(\boldsymbol{r}-\boldsymbol{r}')$ and $g(\cdot):=-Ci(\cdot)\cos(\cdot)-si(\cdot)\sin(\cdot)$, with $si(\cdot)$ and $Ci(\cdot)$ denoting the sine and cosine integrals, respectively (Arfken and Weber, 1995). Applying stationary phase arguments (Bleistein and Handelsman, 1986), one obtains the asymptotic behavior of $\Gamma(\boldsymbol{r},\boldsymbol{r}')$ with $\boldsymbol{r}=r(\cos\varphi,\sin\varphi)$ as $r\to\infty$

$$\Gamma^{\infty}(\boldsymbol{r},\boldsymbol{r}')=\frac{1}{\sqrt{r}}\sum_j B^{+}(u_j^{+})\mathrm{e}^{\mathrm{i}k_{+}(u_j^{+})\hat{\boldsymbol{k}}(u_j^{+})\cdot\boldsymbol{r}}\mathrm{e}^{-\mathrm{i}k_{+}(u_j^{+})\hat{\boldsymbol{k}}(u_j^{+})\cdot\boldsymbol{r}'}+\frac{1}{\sqrt{r}}\sum_j B^{-}(u_j^{-})\mathrm{e}^{\mathrm{i}k_{-}(u_j^{-})\hat{\boldsymbol{k}}(u_j^{-})\cdot\boldsymbol{r}}\mathrm{e}^{-\mathrm{i}k_{-}(u_j^{-})\hat{\boldsymbol{k}}(u_j^{-})\cdot\boldsymbol{r}'}+\mathrm{o}(r^{-1/2}),\tag{97}$$

where $u_j^{\pm}\in(\varphi-\pi/2,\varphi+\pi/2)$ are all the possible stationary points satisfying the equation

$$\tan(u_j^{\pm}-\varphi)=\frac{k_{\pm}'(u_j^{\pm})}{k_{\pm}(u_j^{\pm})},$$

with the prime over $k_{\pm}$ indicating differentiation w.r.t. the argument and $B^{\pm}(u_j^{\pm})$ are specific regular expressions in terms of $u_j^{\pm}$. Given that $\hat{\boldsymbol{k}}(u_j^{\pm})\cdot\boldsymbol{r}=r\cos(u_j^{\pm}-\varphi)>0$, the outgoing behavior of the Green's function is obvious.

Returning to (94), the functions $\mathscr{H}_{\pm}(u)$ can now be considered as the generalized far-field patterns of the scalar field

$$w(\boldsymbol{r}):=\int_{\partial G}\Gamma(\boldsymbol{r},\boldsymbol{r}')h(\boldsymbol{r}')\,\mathrm{d}s(\boldsymbol{r}')+\int_{\partial G}\frac{\partial\Gamma(\boldsymbol{r},\boldsymbol{r}')}{\partial\nu(\boldsymbol{r}')}f(\boldsymbol{r}')\,\mathrm{d}s(\boldsymbol{r}'),\tag{98}$$

or $\boldsymbol{r}\in\mathbb{R}^2\setminus\overline{G}$, which is a combination of two surface potentials. The elastic pair $(U_1(\boldsymbol{r}),U_2(\boldsymbol{r}))$, $\boldsymbol{r}\in\mathbb{R}^2\setminus\overline{G}$ defined by (see Eqs. (34) and (35))

$$U_1(\boldsymbol{r})=-\partial_1\partial_2 w(\boldsymbol{r}),\tag{99}$$

$$U_2(\boldsymbol{r})=(Q_{12}+Q_{66})^{-1}(Q_{11}\partial_1^2+Q_{66}\partial_2^2+\rho\omega^2)w(\boldsymbol{r}),\tag{100}$$

for $\boldsymbol{r}\in\mathbb{R}^2\setminus\overline{G}$ satisfies the coupled system of elasticity equations, propagates outwardly and has zero far-field pattern (Nakamura and Wang, 2004; Natroshvili, 1996). From the generalized Rellich's lemma for anisotropic elasticity (Nakamura and Wang, 2004), we conclude that $(U_1,U_2)=(0,0)$ in $\mathbb{R}^2\setminus G$. With the aid of the definitions (99) and (100), one can show that this also implies $w=0$ in $\mathbb{R}^2\setminus G$, apart indifferent rigid motions.

Having established the result that $w(\boldsymbol{r})$ vanishes identically for $\boldsymbol{r}\notin G$, we proceed by noting that the functions h, f constitute the densities of the layer potentials defined in (98) and therefore can be expressed via suitable jump relations for the field $w(\boldsymbol{r})$ and its normal derivatives across the boundary ∂G. The investigation of these jump relations requires the examination of the emerged boundary integral operators ($\boldsymbol{r}\in\partial G$), which in turn preassumes the knowledge of the asymptotic behavior of the Green's function $\Gamma(\boldsymbol{r},\boldsymbol{r}')$ and its derivatives as $\boldsymbol{r}\to\boldsymbol{r}'\in\partial G$. More precisely, Eq. (96) is subjected to asymptotic analysis for $|\boldsymbol{r}-\boldsymbol{r}'|\to 0$ with the result that

$$\Gamma(\boldsymbol{r},\boldsymbol{r}')=\left[A_1(x_1-x_1')^2+A_2(x_2-x_2')^2\right]\ln|\boldsymbol{r}-\boldsymbol{r}'|+\mathrm{O}(|\boldsymbol{r}-\boldsymbol{r}'|^4\ln|\boldsymbol{r}-\boldsymbol{r}'|),\tag{101}$$

where $A_j=\frac{1}{8(2\pi)^2}I_j$, $j=1,2$ with

$$I_1=\int_0^{2\pi}\frac{\cos^2 u}{D_2(u)}\,\mathrm{d}u,\qquad I_2=\int_0^{2\pi}\frac{\sin^2 u}{D_2(u)}\,\mathrm{d}u.\tag{102}$$

The evaluation of the integrals I_j, $j = 1, 2$ is accomplished by employing complex analysis integration techniques and hence finally reduces to a computation of the residues of specific functions at certain poles lying inside the unit circle in $\mathbb{C}$. We omit the details both for the sake of brevity and since the rest of our analysis does not depend on the exact values of the integrals in (102) in any way.

By use of (101), one can straightforwardly verify the following asymptotic relations, valid for $\boldsymbol{r} \to \boldsymbol{r}' \in \partial G$:

$$\frac{\partial \Gamma(\boldsymbol{r}, \boldsymbol{r}')}{\partial \nu(\boldsymbol{r}')} = 2[A_1(x_1' - x_1)\nu_1' + A_2(x_2' - x_2)\nu_2'] \ln|\boldsymbol{r} - \boldsymbol{r}'| + [A_1 \cos^2\gamma + A_2 \sin^2\gamma]\hat{\boldsymbol{\nu}}' \cdot (\boldsymbol{r}' - \boldsymbol{r}), \tag{103}$$

$$\begin{aligned}\frac{\partial^2 \Gamma(\boldsymbol{r}, \boldsymbol{r}')}{\partial \nu(\boldsymbol{r}) \partial \nu(\boldsymbol{r}')} &= -2[A_1 \nu_1 \nu_1' + A_2 \nu_2 \nu_2'] \ln|\boldsymbol{r} - \boldsymbol{r}'| - 2[A_1 \cos^2\gamma + A_2 \sin^2\gamma]\hat{\boldsymbol{\nu}}' \cdot (\boldsymbol{r}' - \boldsymbol{r}) \frac{\hat{\boldsymbol{\nu}} \cdot (\boldsymbol{r} - \boldsymbol{r}')}{|\boldsymbol{r} - \boldsymbol{r}'|^2} \\ &\quad + 2[A_1(x_1' - x_1)\nu_1' + A_2(x_2' - x_2)\nu_2'] \frac{\hat{\boldsymbol{\nu}} \cdot (\boldsymbol{r} - \boldsymbol{r}')}{|\boldsymbol{r} - \boldsymbol{r}'|^2} + 2[A_1(x_1 - x_1')\nu_1 + A_2(x_2 - x_2')\nu_2] \\ &\quad \times \frac{\hat{\boldsymbol{\nu}}' \cdot (\boldsymbol{r}' - \boldsymbol{r})}{|\boldsymbol{r} - \boldsymbol{r}'|^2} - [A_1 \cos^2\gamma + A_2 \sin^2\gamma]\hat{\boldsymbol{\nu}} \cdot \hat{\boldsymbol{\nu}}',\end{aligned} \tag{104}$$

where γ again denotes the angle between $\boldsymbol{r}$ and $\boldsymbol{r}'$ and the prime indicates a function defined w.r.t. $\boldsymbol{r}'$, e.g., $\hat{\boldsymbol{\nu}}' = (\nu_1', \nu_2') \equiv \hat{\boldsymbol{\nu}}(\boldsymbol{r}')$ is the outward unit normal at the point $\boldsymbol{r}'$ on ∂G. It follows immediately that the corresponding layer potential with kernel given either by (103) or (104) is continuous (Colton and Kress, 1983). In a similar fashion, one can also establish the continuity of the potential with kernel obtained by differentiating (once or twice) $\Gamma(\boldsymbol{r}, \boldsymbol{r}')$ w.r.t. $\hat{\boldsymbol{\nu}}(\boldsymbol{r})$. As will become apparent in the sequel, the jump relations for the layer potentials with kernels involving higher derivatives of the Green's function, namely,

$$\frac{\partial^3 \Gamma(\boldsymbol{r}, \boldsymbol{r}')}{\partial^2 \nu(\boldsymbol{r}) \partial \nu(\boldsymbol{r}')} \quad \text{and} \quad \frac{\partial^3 \Gamma(\boldsymbol{r}, \boldsymbol{r}')}{\partial^3 \nu(\boldsymbol{r})},$$

are also need to be known. It can be shown after extended but straightforward calculations that the limiting behavior of these kernels is of the form

$$\frac{\partial^3 \Gamma(\boldsymbol{r}, \boldsymbol{r}')}{\partial^2 \nu(\boldsymbol{r}) \partial \nu(\boldsymbol{r}')} = -4[A_1 \nu_1 \nu_1' + A_2 \nu_2 \nu_2'] \frac{\partial}{\partial \nu(\boldsymbol{r})} \ln|\boldsymbol{r} - \boldsymbol{r}'| + \Gamma_1^0(\boldsymbol{r}, \boldsymbol{r}'), \tag{105}$$

and

$$\frac{\partial^3 \Gamma(\boldsymbol{r}, \boldsymbol{r}')}{\partial^3 \nu(\boldsymbol{r})} = 4[A_1 \nu_1^2 + A_2 \nu_2^2] \frac{\partial}{\partial \nu(\boldsymbol{r})} \ln|\boldsymbol{r} - \boldsymbol{r}'| + \Gamma_2^0(\boldsymbol{r}, \boldsymbol{r}'), \tag{106}$$

respectively, where $\Gamma_j^0(\boldsymbol{r}, \boldsymbol{r}')$, $j = 1, 2$ constitute functions whose contribution to the jump relations of the corresponding potentials is zero. Hence, the jump relations for the surface potentials $P_1\phi(\boldsymbol{r})$ and $P_2\psi(\boldsymbol{r})$ defined by

$$P_1\phi(\boldsymbol{r}) := \int_{\partial G} \frac{\partial^3 \Gamma(\boldsymbol{r}, \boldsymbol{r}')}{\partial^2 \nu(\boldsymbol{r}) \partial \nu(\boldsymbol{r}')} \phi(\boldsymbol{r}') \, \mathrm{d}s(\boldsymbol{r}'), \quad \boldsymbol{r} \notin G, \tag{107}$$

$$P_2\psi(\boldsymbol{r}) := \int_{\partial G} \frac{\partial^3 \Gamma(\boldsymbol{r}, \boldsymbol{r}')}{\partial^3 \nu(\boldsymbol{r})} \psi(\boldsymbol{r}') \, \mathrm{d}s(\boldsymbol{r}'), \quad \boldsymbol{r} \notin G, \tag{108}$$

can be determined by the corresponding relations valid for the logarithmic single-layer potential $\mathrm{SL}\phi(\boldsymbol{r})$ defined as (see McLean, 2000)

$$\mathrm{SL}\phi(\boldsymbol{r}) = \frac{1}{2\pi}\int_{\partial G} \ln\frac{1}{|\boldsymbol{r}-\boldsymbol{r}'|}\phi(\boldsymbol{r}')\,\mathrm{d}s(\boldsymbol{r}'), \quad \boldsymbol{r}\notin G. \tag{109}$$

Using the notation $[v]_{\partial G}$ to denote the jump $\gamma_0^+ v - \gamma_0^- v$ across ∂G and the well-known jump relation $[\frac{\partial}{\partial \nu}\mathrm{SL}\phi]_{\partial G} = -\phi$, one can easily arrive at

$$[P_1\phi]_{\partial G} = -8\pi(A_1 v_1^2 + A_2 v_2^2)\phi \quad \text{and} \quad [P_2\psi]_{\partial G} = 8\pi(A_1 v_1^2 + A_2 v_2^2)\psi. \tag{110}$$

With the foregoing results at hand, we can now return to relation (98) and, with the aid of (103) and (104) (see also the discussion following these relations), conclude that $[w]_{\partial G} = 0$ and $\left[\frac{\partial w}{\partial \nu}\right]_{\partial G} = 0$. Since we have shown that $w = 0$ in $\mathbb{R}^2 \setminus G$, the relations $\gamma_0^- w = \gamma_1^- w = 0$ on ∂G follow. In addition, Eq. (98) implies that $Lw(\boldsymbol{r}) = 0$ for $\boldsymbol{r}\in G$. In other words, the field w satisfies the homogeneous BVP

$$Lw = 0 \quad \text{in } G, \tag{111}$$

$$\gamma_0^- w = \gamma_1^- w = 0 \quad \text{on } \partial G, \tag{112}$$

where the set of boundary conditions forms a normal Dirichlet system of order 2 (Wloka, 1987). It can be verified that the operator L is properly elliptic if and only if the relation $2Q_{66} > \sqrt{Q_{11}Q_{22}} - Q_{12}$ holds between the elastic stiffness coefficients. Assuming that the operator L possesses this property, one can conclude that the BVP (111) and (112) satisfies the conclusions of the Riesz-Schauder spectral theorem (Wloka, 1987), according to which w vanishes identically in G, provided that the frequency ω does not belong to the discreet set of eigenvalues of the specific BVP. Now, from the one hand, the vanishing of the field w in G (and in $\mathbb{R}^2 \setminus G$ also) implies that $\left[\frac{\partial^2 w}{\partial \nu^2}\right]_{\partial G} = 0$ while, on the other hand, the jump relation for the layer potential $\frac{\partial^2 w}{\partial \nu^2}$, obtained by differentiating (98), is

$$\left[\frac{\partial^2 w}{\partial \nu^2}\right]_{\partial G} = [P_1 f]_{\partial G} = -8\pi(A_1 v_1^2 + A_2 v_2^2)f, \tag{113}$$

due to the first relation in (110) and the continuity of the potential with kernel $\frac{\partial^2 \Gamma(\boldsymbol{r},\boldsymbol{r}')}{\partial \nu^2(\boldsymbol{r})}$. Hence, the density function f must vanish and therefore the field w 'reduces' to

$$w(\boldsymbol{r}) = \int_{\partial G} \Gamma(\boldsymbol{r},\boldsymbol{r}')h(\boldsymbol{r}')\,\mathrm{d}s(\boldsymbol{r}'), \quad \boldsymbol{r}\notin \partial G. \tag{114}$$

In a similar fashion, one can see that the vanishing jump of the surface potential $\frac{\partial^3 w}{\partial \nu^3}$ obtained by differentiating (114) under the integral sign (for $\boldsymbol{r}\in G$) implies the vanishing of the function h since, by the second relation in (110), it holds that

$$\left[\frac{\partial^3 w}{\partial \nu^3}\right]_{\partial G} = [P_2 h]_{\partial G} = 8\pi(A_1 v_1^2 + A_2 v_2^2)h. \tag{115}$$

Thus we have shown that the functions f and h both vanish and this completes the proof of the denseness of the space $\mathscr{R}$ in X. We are in a position now to obtain the main result of this Appendix, that is, the closure of $\mathscr{Q}$ in $H^2(G)$ coincides with $\overline{\mathscr{W}(G)}$. This result is an immediate consequence of the fact that the version of the BVP (111) and (112) with nonhomogeneous boundary conditions is well-posed. More precisely, for every given pair of boundary data $(f_0, h_0)\in X$, the BVP

$$Lv = 0 \quad \text{in } G, \tag{116}$$

$$\left.\begin{aligned}\gamma_0^- v &= f_0\\ \gamma_1^- v &= h_0\end{aligned}\right\} \quad \text{on } \partial G, \tag{117}$$

possesses a unique solution $v\in H^2(G)$ provided that ω is not an eigenvalue of the corresponding Dirichlet problem. This solution depends continuously on the given data in the sense that

$$\|v\|_{H^2(G)} \leqslant C\big(\|f_0\|_{H^{3/2}(\partial G)} + \|h_0\|_{H^{1/2}(\partial G)}\big), \tag{118}$$

holds for some positive constant C. Since (f_0, h_0) can be approximated arbitrary closely in the norm of X by $(\gamma_0^- \phi, \gamma_1^- \phi)$ with $\phi \in \mathcal{Q}$, the approximation of the function v by ϕ in $H^2(G)$ follows from (118) and this proves our main assertion.

To finish our discussion, we wish to point out that an alternative approach to proving the desired denseness result is offered by the methodology originally proposed in Colton and Kress (2001) for the case of far-field acoustics and electromagnetics and adopted in Nintcheu Fata and Guzina (2004) for the near-field elastodynamics case. This approach is based on variational methods and has the potential advantage of avoiding the problems concerned with eigenvalues. However, the price paid for the latter advantage, is an increment of the complexity of the whole approach compared with the one presented here. Such an approach will be the subject matter of a future work.

Appendix B

The explicit expressions for $D_m^t(r,\varphi)$, $Z_m^t(r,\varphi)$, $t = r, \varphi$ in Eq. (67) are

$$D_m^r(r,\varphi) := 2\mu e^{im\varphi}\left\{ v_r\left[-\frac{H_m^{(1)'}\left(k_p^{ext} r\right)}{r} - k_p^{ext}\left(1 + \frac{\lambda}{2\mu} - \frac{m^2}{(k_p^{ext} r)^2}\right) H_m^{(1)}(k_p^{ext} r)\right]\right.$$
$$\left. + v_\varphi\left[im\left(\frac{H_m^{(1)'}(k_p^{ext} r)}{r} - \frac{H_m^{(1)}(k_p^{ext} r)}{k_p^{ext} r^2}\right)\right]\right\},$$

$$D_m^\varphi(r,\varphi) := 2\mu e^{im\varphi}\left\{ v_r\left[im\left(\frac{H_m^{(1)'}(k_p^{ext} r)}{r} - \frac{H_m^{(1)}(k_p^{ext} r)}{k_p^{ext} r^2}\right)\right]\right.$$
$$\left. + v_\varphi\left[\frac{H_m^{(1)'}(k_p^{ext} r)}{r} - \left(\frac{\lambda k_p^{ext}}{2\mu} + \frac{m^2}{k_p^{ext} r^2}\right) H_m^{(1)}(k_p^{ext} r)\right]\right\},$$

$$Z_m^r(r,\varphi) := 2\mu e^{im\varphi}\left\{ v_r\left[im\left(\frac{H_m^{(1)'}(k_s^{ext} r)}{r} - \frac{H_m^{(1)}(k_s^{ext} r)}{k_s^{ext} r^2}\right)\right]\right.$$
$$\left. + v_\varphi\left[\frac{H_m^{(1)'}(k_s^{ext} r)}{r} + \left(\frac{k_s^{ext}}{2} - \frac{m^2}{k_s^{ext} r^2}\right) H_m^{(1)}(k_s^{ext} r)\right]\right\}$$

$$Z_m^\varphi(r,\varphi) := 2\mu e^{im\varphi}\left\{ v_r\left[\frac{H_m^{(1)'}(k_s^{ext} r)}{r} + k_s^{ext}\left(\frac{1}{2} - \frac{m^2}{(k_s^{ext} r)^2}\right) H_m^{(1)}(k_s^{ext} r)\right]\right.$$
$$\left. + v_\varphi\left[im\left(\frac{H_m^{(1)}(k_s^{ext} r)}{k_s^{ext} r^2} - \frac{H_m^{(1)'}(k_s^{ext} r)}{r}\right)\right]\right\},$$

where v_r, v_φ are the polar coordinates of the outward unit normal $\hat{\boldsymbol{v}}$ on ∂G and the prime denotes differentiation with respect to the argument.

The quantities $F^{\pm}_{m'}(r,\varphi)$ and $F^{\pm}_{m'}(r,\varphi)$ entering Eq. (68) are determined by

$$F^{\pm}_{m'}(r,\varphi) := \left\{ \frac{\mathrm{i}^{-(m'+1)}}{M} \sum_{j=1}^{M} \left\{ \left\{ k^3_{\pm}(u_j)\cos u_j \sin u_j [v_1 Q_{11}\cos u_j + v_2 Q_{66}\sin u_j] + \frac{k_{\pm}(u_j)}{Q_{12}+Q_{66}} \left[v_1 Q_{12}\sin u_j + v_2 Q_{66}\cos u_j \right] \left[\rho\omega^2 - k^2_{\pm}(u_j) \left(Q_{11}\cos^2 u_j + Q_{66}\sin^2 u_j \right) \right] \right\} \mathrm{e}^{-\mathrm{i}k_{\pm}(u_j) r\cos(\varphi-u_j)} \mathrm{e}^{\mathrm{i}m' u_j} \right\} \right\},$$

$$G^{\pm}_{m'}(r,\varphi) := \left\{ \frac{\mathrm{i}^{-(m'+1)}}{M} \sum_{j=1}^{M} \left\{ \left\{ k^3_{\pm}(u_j)\cos u_j \sin u_j [v_1 Q_{66}\sin u_j + v_2 Q_{12}\cos u_j] + \frac{k_{\pm}(u_j)}{Q_{12}+Q_{66}} [v_1 Q_{66}\cos u_j + v_2 Q_{22}\sin u_j] \left[\rho\omega^2 - k^2_{\pm}(u_j) \left(Q_{11}\cos^2 u_j + Q_{66}\sin^2 u_j \right) \right] \right\} \mathrm{e}^{-\mathrm{i}k_{\pm}(u_j) r\cos(\varphi-u_j)} \mathrm{e}^{\mathrm{i}m' u_j} \right\} \right\},$$

where v_1, v_2 are the Cartesian components of $\hat{\boldsymbol{v}}$ on ∂G.

The explicit expressions for the elements ${}^{(j)}B^{s}_{m,n}$, $s = \{A^{\mathrm{ext}}, B^{\mathrm{ext}}\}$, $j = 1,2,3,4$ are

$${}^{(1)}B^{A^{\mathrm{ext}}}_{m,n} := \left\{ \left[H^{(1)'}_m(k^{\mathrm{ext}}_{\mathrm{p}} r)\cos\varphi - \frac{\mathrm{i}m}{k^{\mathrm{ext}}_{\mathrm{p}} r} H^{(1)}_m(k^{\mathrm{ext}}_{\mathrm{p}} r)\sin\varphi \right] \mathrm{e}^{\mathrm{i}m\varphi} \right\}_{|(r_n,\varphi_n)},$$

$${}^{(1)}B^{B^{\mathrm{ext}}}_{m,n} := \left\{ \left[\frac{\mathrm{i}m}{k^{\mathrm{ext}}_{\mathrm{s}} r} H^{(1)}_m(k^{\mathrm{ext}}_{\mathrm{s}} r)\cos\varphi + H^{(1)'}_m(k^{\mathrm{ext}}_{\mathrm{s}} r)\sin\varphi \right] \mathrm{e}^{\mathrm{i}m\varphi} \right\}_{|(r_n,\varphi_n)},$$

$${}^{(2)}B^{A^{\mathrm{ext}}}_{m,n} := \left\{ \left[H^{(1)'}_m(k^{\mathrm{ext}}_{\mathrm{p}} r)\sin\varphi + \frac{\mathrm{i}m}{k^{\mathrm{ext}}_{\mathrm{p}} r} H^{(1)}_m(k^{\mathrm{ext}}_{\mathrm{p}} r)\cos\varphi \right] \mathrm{e}^{\mathrm{i}m\varphi} \right\}_{|(r_n,\varphi_n)},$$

$${}^{(2)}B^{B^{\mathrm{ext}}}_{m,n} := \left\{ \left[\frac{\mathrm{i}m}{k^{\mathrm{ext}}_{\mathrm{s}} r} H^{(1)}_m(k^{\mathrm{ext}}_{\mathrm{s}} r)\sin\varphi - H^{(1)'}_m(k^{\mathrm{ext}}_{\mathrm{s}} r)\cos\varphi \right] \mathrm{e}^{\mathrm{i}m\varphi} \right\}_{|(r_n,\varphi_n)},$$

$${}^{(3)}B^{A^{\mathrm{ext}}}_{m,n} := D^{r}_{m}(r_n,\varphi_n)\cos\varphi_n - D^{\varphi}_{m}(r_n,\varphi_n)\sin\varphi_n,$$

$${}^{(3)}B^{B^{\mathrm{ext}}}_{m,n} := Z^{r}_{m}(r_n,\varphi_n)\cos\varphi_n - Z^{\varphi}_{m}(r_n,\varphi_n)\sin\varphi_n,$$

$${}^{(4)}B^{A^{\mathrm{ext}}}_{m,n} := D^{r}_{m}(r_n,\varphi_n)\sin\varphi_n + D^{\varphi}_{m}(r_n,\varphi_n)\cos\varphi_n,$$

$${}^{(4)}B^{B^{\mathrm{ext}}}_{m,n} := Z^{r}_{m}(r_n,\varphi_n)\sin\varphi_n + Z^{\varphi}_{m}(r_n,\varphi_n)\cos\varphi_n,$$

and for the elements ${}^{(j)}B^{t}_{m',n}$, $t = \{A^{+}, A^{-}\}$, $j = 1,2,3,4$ are

$${}^{(1)}B^{A^{\pm}}_{m',n} := -\left\{ \frac{\mathrm{i}^{-m'}}{M} \sum_{j=1}^{M} \left\{ k^2_{\pm}(u_j)\sin u_j \cos u_j \mathrm{e}^{-\mathrm{i}k_{\pm}(u_j) r\cos(\varphi-u_j)} \mathrm{e}^{\mathrm{i}m' u_j} \right\} \right\}_{|(r_n,\varphi_n)},$$

$${}^{(2)}B^{A^{\pm}}_{m',n} := -\left\{ \frac{\mathrm{i}^{-m'}}{M} \sum_{j=1}^{M} \left\{ \frac{1}{Q_{12}+Q_{66}} \left[\rho\omega^2 - k^2_{\pm}(u_j) \left(Q_{11}\cos^2 u_j + Q_{66}\sin^2 u_j \right) \right] \mathrm{e}^{-\mathrm{i}k_{\pm}(u_j) r\cos(\varphi-u_j)} \mathrm{e}^{\mathrm{i}m' u_j} \right\} \right\}_{|(r_n,\varphi_n)},$$

$${}^{(3)}B^{A^{\pm}}_{m',n} := -F^{\pm}_{m'}(r_n,\varphi_n),$$

$${}^{(4)}B^{A^{\pm}}_{m',n} := -G^{\pm}_{m'}(r_n,\varphi_n).$$

References

Arfken, G.B., Weber, H.J., 1995. Mathematical Methods for Physicists, fourth ed. Academic Press, San Diego.

Ben-Menahem, A., Singh, S.J., 1981. Seismic Waves and Sources. Springer-Verlag, New York.

Bleistein, N., Handelsman, R.A., 1986. Asymptotic Expansions of Integrals. Dover Publications, Inc., New York.

Charalambopoulos, A., 2002. On the interior transmission problem in nondissipative, inhomogeneous, anisotropic elasticity. Journal of Elasticity 67, 149–170.

Colton, D., Kress, R., 1983. Integral Equation Methods in Scattering Theory. Wiley-Interscience, New York.

Colton, D., Kress, R., 1992. Inverse Acoustic and Electromagnetic Scattering Theory. Springer-Verlag, Berlin.

Colton, D., Kress, R., 2001. On the denseness of Herglotz wave functions and electromagnetic Herglotz pairs in Sobolev spaces. Mathematical Methods in the Applied Sciences 24, 1289–1303.

Dassios, G., Kiriaki, K., Polyzos, D., 1995. Scattering theorems for complete dyadic fields. International Journal of Engineering Science 33 (2), 269–277.

Fellinger, P., Marklein, R., Langenberg, K.J., Klaholz, S., 1995. Numerical modeling of elastic wave propagation and scattering with EFIT—Elastodynamic finite integration technique. Wave Motion 21, 47–66.

Honarvar, F., Sinclair, A.N., 1996. Acoustic wave scattering from transversely isotropic cylinders. Journal of the Acoustical Society of America 100, 57–63.

Jones, R.M., 1975. Mechanics of Composite Materials. McGraw-Hill, Tokyo.

Kim, J.-Y., Ih, J.-G., 2003. Scattering of plane acoustic waves by a transversely isotropic cylindrical shell-application to material characterization. Applied Acoustics 64, 1187–1204.

Kundu, T., Boström, A., 1992. Elastic wave scattering by a circular crack in a transversely isotropic solid. Wave Motion 15, 285–300.

Kupradze, V.D., 1979. Three-dimensional Problems of the Mathematical Theory of Elasticity and Thermoelasticity. North-Holland, Amsterdam.

Leis, R., 1986. Initial Boundary Value Problems in Mathematical Physics. John Wiley & Sons Ltd. and B.G. Teubner, Stuttgart.

Liu, G.R., Achenbach, J.D., 1995. Strip element method to analyze wave scattering by cracks in anisotropic laminated plates. Journal of Applied Mechanics 62, 607–613.

Lord, W., Ludwig, R., You, Z., 1990. Developments in ultrasonic modeling with finite element analysis. Journal of Nondestructive Evaluation 9, 129–143.

Mal, A.K., Yin, C.-C., Bar-Cohen, Y., 1992. Analysis of acoustic pulses reflected from fiber reinforced composite laminates. Journal of Applied Mechanics 59, S136–S144.

Mattsson, J., 1994. Ultrasonic 2D-SH wave scattering by interface flaws in anisotropic solid media. Report (1), Div. Mech., Chalmers Univ. Tech., Göteborg, Sweden.

Mattsson, J., 1995. 2D in-plane ultrasonic scattering by a strip-like flaw in an anisotropic solid. Report (3), Div. Mech., Chalmers Univ. Tech., Göteborg, Sweden.

McLean, W., 2000. Strongly Elliptic Systems and Boundary Integral Equations. Cambridge University Press, Cambridge.

Morse, P.M., Feshbach, H., 1953. Methods of Theoretical Physics, vol. II. McGraw-Hill, New York.

Nakamura, G., Wang, J.-N., 2004. The limiting absorption principle for the two-dimensional inhomogeneous anisotropic elasticity system. Transactions of the American Mathematical Society, December 2004.

Natroshvili, D., 1996. Two-dimensional steady-state oscillation problems of anisotropic elasticity. Georgian Mathematical Journal 3, 239–262.

Niklasson, A.J., Datta, S.K., 1998. Scattering by an infinite transversely isotropic cylinder in a transversely isotropic medium. Wave Motion 27, 169–185.

Nintcheu Fata, S., Guzina, B.B., 2004. A linear sampling method for near-field inverse problems in elastodynamics. Inverse Problems 20, 713–736.

Polyzos, D., Tsinopoulos, S.V., Beskos, D.E., 1998. Static and dynamic boundary element analysis in incompressible linear elasticity. European Journal of Mechanics and Solids 17, 515–536.

Rajapakse, R.K.N.D., Gross, D., 1995. Transient response of an orthotropic elastic medium with a cavity. Wave Motion 21, 231–252.

Verbis, J.T., Kattis, S.E., Tsinopoulos, S.V., Polyzos, D., 2001. Wave dispersion and attenuation in fiber composites. Computational Mechanics 27, 244–252.

Wang, C.-Y., Achenbach, J.D., Hirose, S., 1996. Two-dimensional time domain BEM for scattering of elastic waves in solids of general anisotropy. International Journal of Solids and Structures 33, 3843–3864.

Wloka, J., 1987. Partial Differential Equations. Cambridge University Press, Cambridge.